Table 1 Effects of treatment with G-CSF for 10 days on physiological parameters at 6 weeks after MI in anesthetized dogs

	Sham	Myocardial infarction		P value
		Control	GCSF	
n	4	10	13	
BW (kg)	11.7±0.1	10.1±0.2*	10.6±0.2	0.0875
SBP (mmHg)	118±7	113±5	110±3	0.6634
DBP (mmHg)	95±4	91±4	90±3	0.9047
HR (bpm)	161±12	135±7	146±4	0.1752
LVSP (mmHg)	124±3	108±4*	107±3	0.8894
LVEDP (mmH)	5±1	7±1	5±1	0.2798
LVdP/dt (mmHg/s)	3017±281	2367±237	2329±108	0.8887
-LVdP/dt (mmHg/s)	2996±184	2517±130	2700±134	0.3382
CO (L/min)	1.8±0.1	1.4±0.1*	1.6±0.1	0.3195
PAP (mmHg)	19±1	20±1	18±0	0.1853
pH	7.407±0.010	7.405±0.007	7.394±0.006	0.2334
pCO_2 (mmHg)	35.2±1.6	34.2±0.7	34.9±0.8	0.5053
pO_2 (mmHg)	123.1±4.7	116.4±2.0	115.1±2.2	0.6479
BT (℃)	35.9±0.1	36.5±0.2	36.5±0.1	0.9831

Values are expressed as mean ±SEM. BW: body weight, SBP: systolic arterial blood pressure, DBP: diastolic arterial blood pressure, HR: heart rate, LVSP: left ventricular (LV) systolic pressure, LVEDP: LV end diastolic pressure, LVdP/dt(+) and (-) : maximal and minimal first derivative of LV pressure, CO: cardac output, PAP: mean pulmonary arterial blood pressure, BT: body temperature.

Table 2 Effects of treatment with G-CSF for 10 days on infarct size, cardiac weight, and echocardiographic parameters at 6weeks after MI in anesthetized dogs

	Sham	Myocardial infarction		P value
		Control	G-CSF	
n	4	10	13	
BW (kg)	11.7±0.1	10.1±0.2	10.6±0.2	0.0875
Infarct size	0.012±0.012	0.132±0.011*	0.133±0.009	0.7963
LVW (g)	63.8±3.0	52.6±1.5*	54.5±1.7	0.3988
RVW (g)	21.3±0.6	19.3±0.7	19.6±0.8	0.7965
LVEDD (mm)	21.7±1.9	32.2±0.9*	33.5±0.8	0.2831
LVESD (mm)	12.9±3.1	26.0±0.8*	28.1±0.7	0.0793
HR (bpm)	157±13	138±7	147±4	0.1752
FS	0.42±0.10	0.19±0.02*	0.16±0.02	0.2241
EF	0.71±0.11	0.40±0.03*	0.34±0.03	0.1592

Values are expressed as mean ± SEM. BW: body weight, LVW: left ventricle weight, RVW: right ventricle weight; LVEDD: left ventricular end diastolic dimension, LVESD: left ventricular end systolic dimension, HR: heart rate, FS: fractional shortening, EF: ejection fraction.

Hemodynamic measurements and echocardiogram

Hemodynamic analysis performed at 6 weeks was shown in Table 1. Cardiac output was not significantly different between the control and G-CSF groups. LVEDP seemed to have a tendency to decrease in G-CSF group, but not significant. There was no significant difference between the two groups in other hemodynamic parameters such as body weight, systolic and diastolic blood pressure, LV end-diastolic pressure, pulmonary artery pressure, pH, pCO_2, pO_2, and body temperature.

Echocardiographic measurements were shown in Table 2. There was no significant difference in LV end-diastolic dimension, LV end-systolic dimension, heart rate, fractional shortening and ejection fraction between the two groups. These findings indicated that G-CSF administration did not improve or aggravate the cardiac function after MI.

Macroscopic findings of LV

Anatomical measurement had revealed that there was no difference in LV weight, RV weight and infarcted size between the two groups. Infarct size did not differ between the two groups (Table 2). Fig. 2 revealed the representative photograph of the LV slices at papillary muscle level. Using these LV slices, we investigated LV dimension and infracted wall thickness. There were no significant differences between the groups in LV dimension. However, the infracted wall thickness was significantly greater in G-CSF group, implying that G-SCF might affect the cardiac remodeling after myocardial infarction.

Histological analysis

Since G-CSF can mobilize bone marrow derived cells into peripheral blood, we next investigated the cellular density of the infarcted area. Fig. 3 A-D showed the representative photograph of the azan staining of the infarcted area. Red area indicated the cellular component and blue indicated the interstitial tissue. In both endocardium and epicardium, the red area in the G-CSF treated group seemed to be greater than that of the control group. Quantitative analysis of the red-stained area in both groups was shown in Fig. 3 E,F. The red-stained area of the epicardial layer in G-CSF group was significantly bigger than that of the control group. The red-stained area of the endocardial layer in G-CSF group had a tendency to be bigger than the control group, but it was not statistically significant.

Immunohistochemical analysis

To further investigate the infarcted tissue, we performed immunostaining. Fig. 4 A-D indicated the representative photograph of the nuclear staining with Toto-3. Fig. 4 E,F showed the quantitative analysis of the cell density in the infarcted area. The cell density of both the epicardial and endocardial layer in G-CSF group was significantly higher than those of the control groups. Together with the results of Fig. 3, G-CSF significantly increased the number of cells in the infarcted area.

Fig. 5 A-D showed the representative immunofluorescent microscopy of the infarcted tissue in the control and G-CSF groups with anti-α-SMA antibody. The α-SMA was also expressed in the myofibroblasts in the infarcted area as well as smooth muscle cells. Quantitative analysis of the density of α-SMA-positive cells was shown in Fig. 5 E,F. G-CSF significantly increased the number of α-SMA-positive cells of the epicardial layer and had a tendency to increase that of the epicardial layer in G-CSF group than those in the control groups.

Fig. 6 A-D showed the representative immunofluorescent microscopy of the infarcted area stained with anti-CD31 (PECAM-1) antibody. Quantitative analysis of

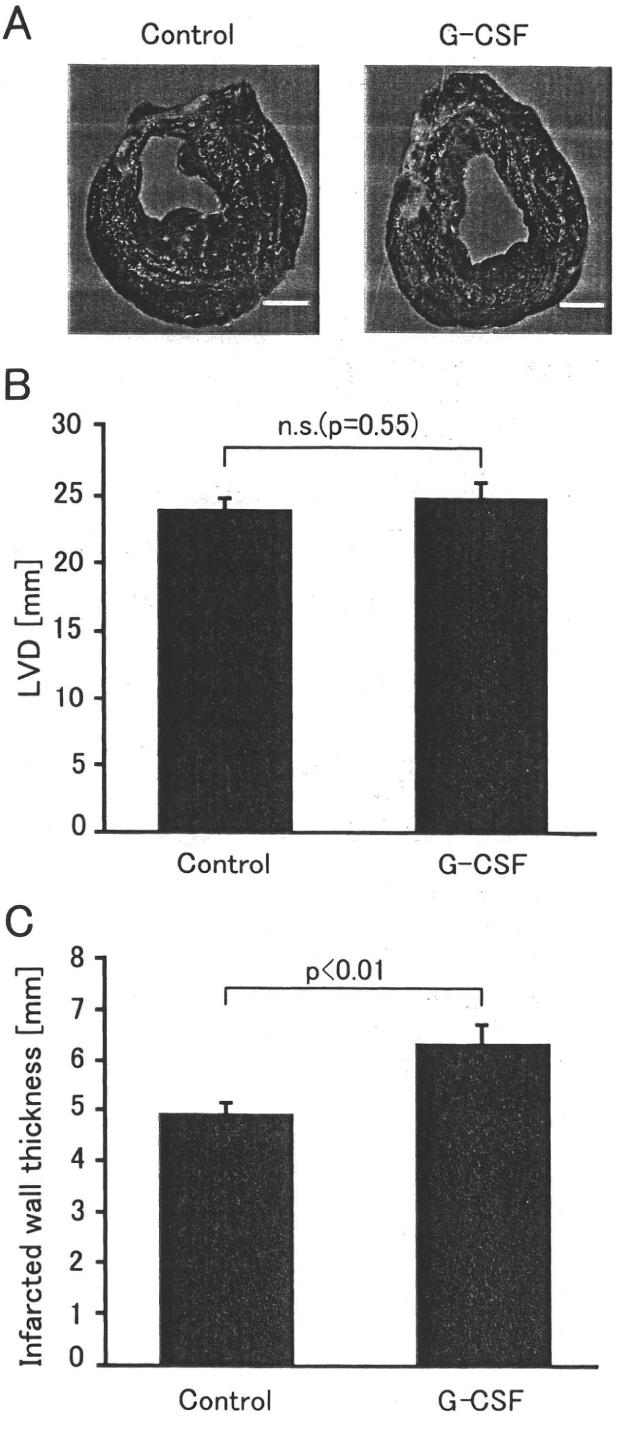

Fig. 2 Effect of G-CSF on left ventricular dimension (LVD) and infarcted wall thickness.

(A) Representative photograph of the slice of infarcted heart at the papillary muscle level in short axis view. Scale bars show 1 cm. (B) LVD of the control and the G-CSF groups was shown. Data were obtained from 10 (Control) and 13 (G-CSF) dogs, respectively. (C) Wall thickness of the infarcted area was shown. Data were obtained from 10 (Control) and 13 (G-CSF) dogs, respectively. Note that wall thickness in G-CSF group was significantly bigger than that of the control group.

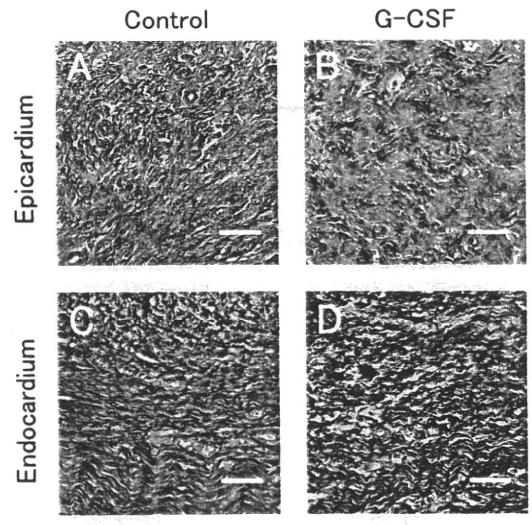

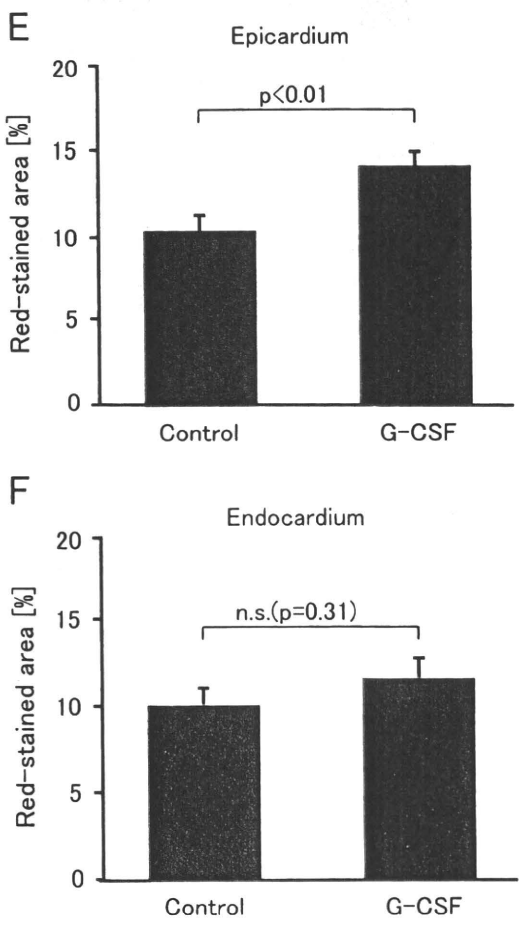

Fig. 3 G-CSF increased the cellular component in the infarcted area

(A-D) Representative microphotograph of the Azan staining of the infarcted area. Blue indicated extracellular matrix and red indicated cellular component. Note that red area was increased by G-CSF administration. Scale bars showed 200 μm. (E, F) Quantative analysis of the red stained area was shown. E and F showed epicardial and endocardial layer, respectively. G-CSF significantly increased the cellular component in the epicardial layer.

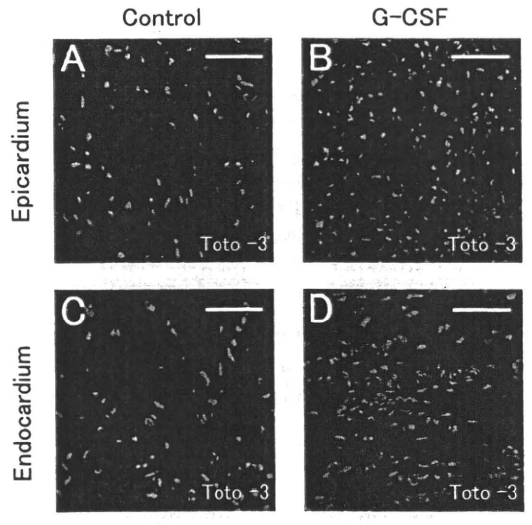

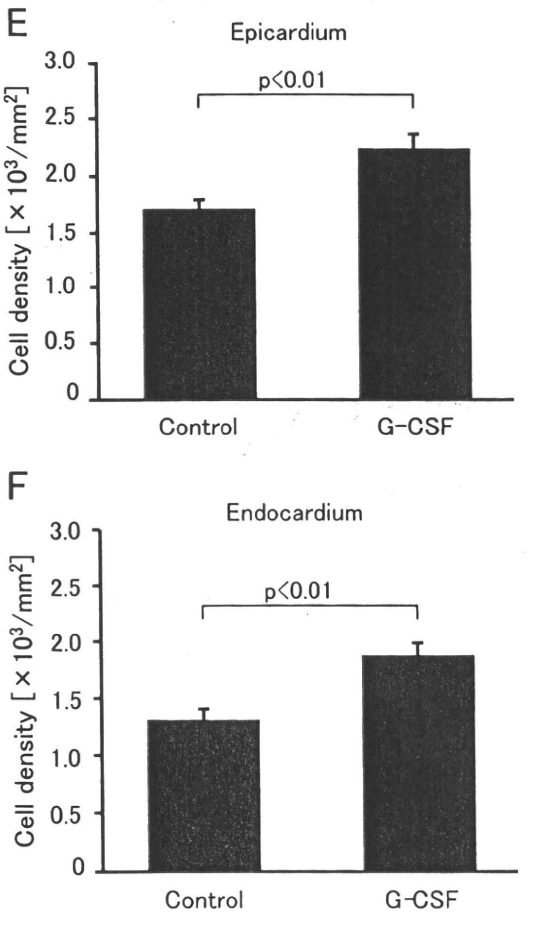

Fig. 4 G-CSF increased the cell number in the infarcted area.

(A-D) Representative microphotograph of the infarcted area by Toto-3, by which nucleus was specifically stained. Scale bars showed 50 μm. (E, F) The cell number in the infarcted area was quatitated. E and F showed epicardial and endocardial layer, respectively. G-CSF significantly increased the cell number in the infarcted area in both epicardial and endocardial layer.

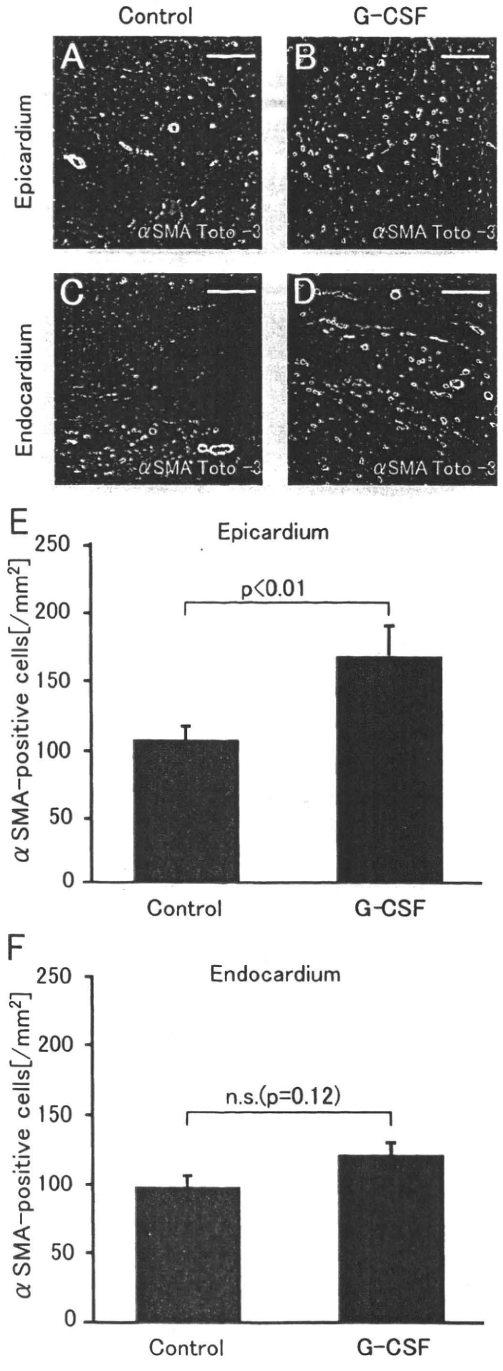

Fig. 5 G-CSF increased the number of α-smooth muscle actin(+) cells in the infarcted area.

(A-D) Epicardial and endocardial layer of the infarced area was separately shown in the control and G-CSF treated groups. Green and blue signals indicated α-smooth muscle actin (α-SMA) (+) and nuclei, respectively. Scale bars show 200μm. (E, F) The number of α-SMA(+) cells of the infarcted area was obtained with immunofluorescent staining, quantiated by NIH image and shown in E and F. Vessel density of the epicardial layer in G-CSF group was significantly higher than that of the control. The number of α-SMA(+) cells of the endocardial layer in G-CSF group has a tendency to be higher than that the control group, but was not statistically significant.

the CD31-positive cell density of the infarcted area was shown in Fig. 6 E,F. G-CSF significantly increased the number of CD31-positive cells of the epicardial layer and had a tendency to increase those of the endocardial layer in G-CSF than those of the control groups. These findings indicated that G-CSF increased the number of endothelial cells, smooth muscle cells and fibroblasts.

Fig. 7 A-D indicated the representative photograph of the infarcted area stained with anti-actinin antibody, and Fig. 7 E,F showed the quantitative analysis. As it is well known, the cardiomyocytes was spared at the subendocardial and subepicardial layer. G-CSF did not significantly affect the survived cardiomyocyte at the epicardial and endocardial layers. G-CSF did not significantly increase the number of cardiomyocytes in the infarcted area. These findings indicated that the survived or regenerated cardiomyocytes were not increased by the administration of G-CSF at the statistically significant level.

Fig. 8 A-D indicated the representative photograph of the infarcted area stained with vimentin antibodies, and Fig. 8 E,F showed the quantitative analysis. G-CSF administration slightly increased the number of vimentin positive cells in the epicardium, although it is not significant. Taken together, these findings indicated that G-CSF administration slightly increased the density of endothelial cells, smooth muscle cells, and fibroblasts in the infarcted area, and its tendency was observed especially at the epicardium.

Discussion

We previously showed that mesenchymal stem cells, not hematopoietic stem cells, could differentiate into cardiomyocytes *in vivo* after MI.[20] We also reported that bone marrow derived cells can both transdifferentiate into and fuse with cardiomyocytes in pressure overloaded heart using murine pulmonary hypertention and transaortic constriction model.[21] However, the significance of this phenomenon with respect to the G-CSF-induced improvement of cardiac function and survival after MI was not determined. This is due to the fact that the number of regenerated cardiomyocytes was very few even G-CSF was administered, and that it is difficult to explain the beneficial effect of G-CSF to be regenerated cardiomyocytes. Since the fundamental effect of G-CSF was to mobilize the granulocytes and monocytes into peripheral circulation, these cells might infiltrate into the infarcted area.

We recently performed BM transplantation using GFP-transgenic mice as a donor, and investigated the contribution of hematopoietic stem cells -derived cells to the healing process after MI in mice.[22] We found that many hematopoietic stem cell-derived cells, which have a fibroblast-like elongated morphology, are retained at the infarcted myocardium at 7 days post-MI. These cells

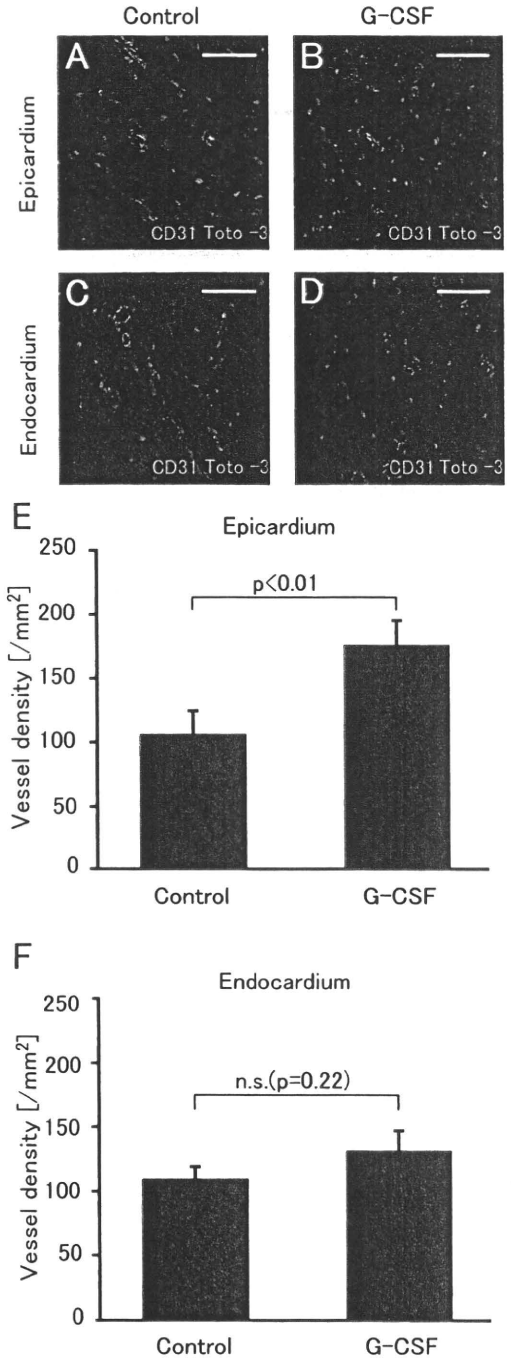

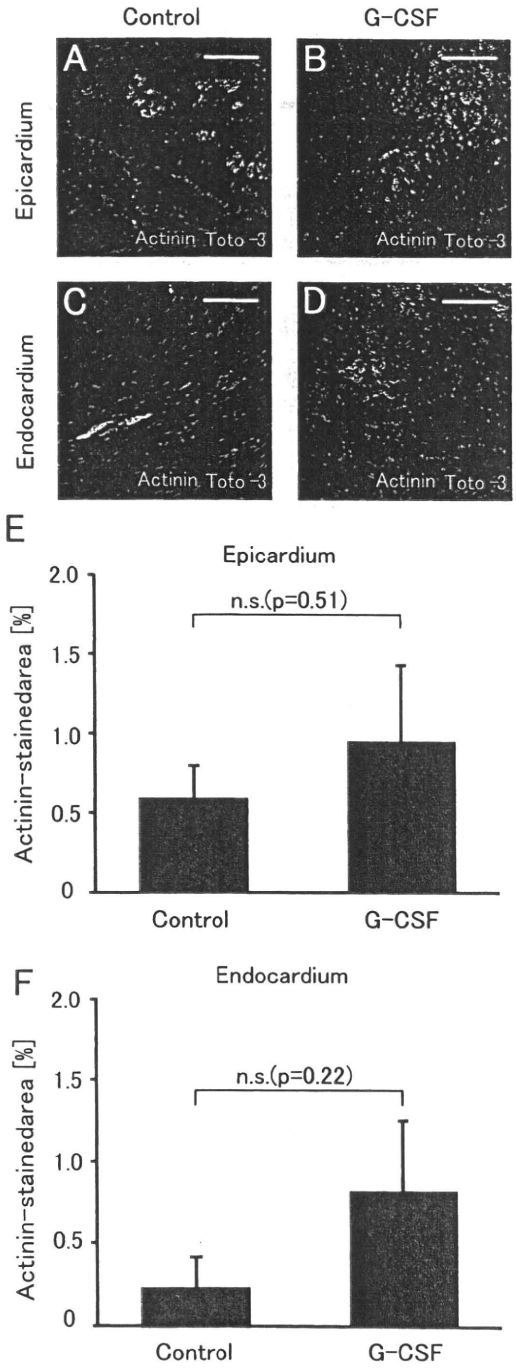

Fig. 6 G-CSF increased the number of CD31(+) cells in the infarcted area.

(A-D) Epicardial and endocardial layer of the infarced area was separately shown in the control and G-CSF treated groups. Green and blue signals indicated CD31 and nuclei, respectively. Scale bars show 50μm. (E, F) The number of CD31(+) cells of the infarcted area was obtained with immunofluorescent staining, quantiated by NIH image and shown in E and F. CD31(+) cell density of the epicardial layer in G-CSF group was significantly higher than that of the control. CD31(+) cell density of the endocardial layer in G-CSF group has a tendency to be higher than that the control group, but was not statistically significant.

Fig. 7 Immunofluorescent staining for actinin on the infarcted area

(A)~(D) Representative immunofluorescent microphotograph of the infarcted area using cardiac actinin antibody. (A, B) Comparison of the endocardium between control (A) and G-CSF group (B). (C, D) Comparison of the epicardium between control (C) and G-CSF group (D). Blue = Nuclei stained by TOTO-3. Scale bars show 50μm. (E, F) The actinin-positive cell density in the endocardium (E) and the epicardium (F). The actinin-positive cell density of G-CSF group had a tendency to be greater than that of the control group in both endocardium and epicardium, although it was not statistically significant.

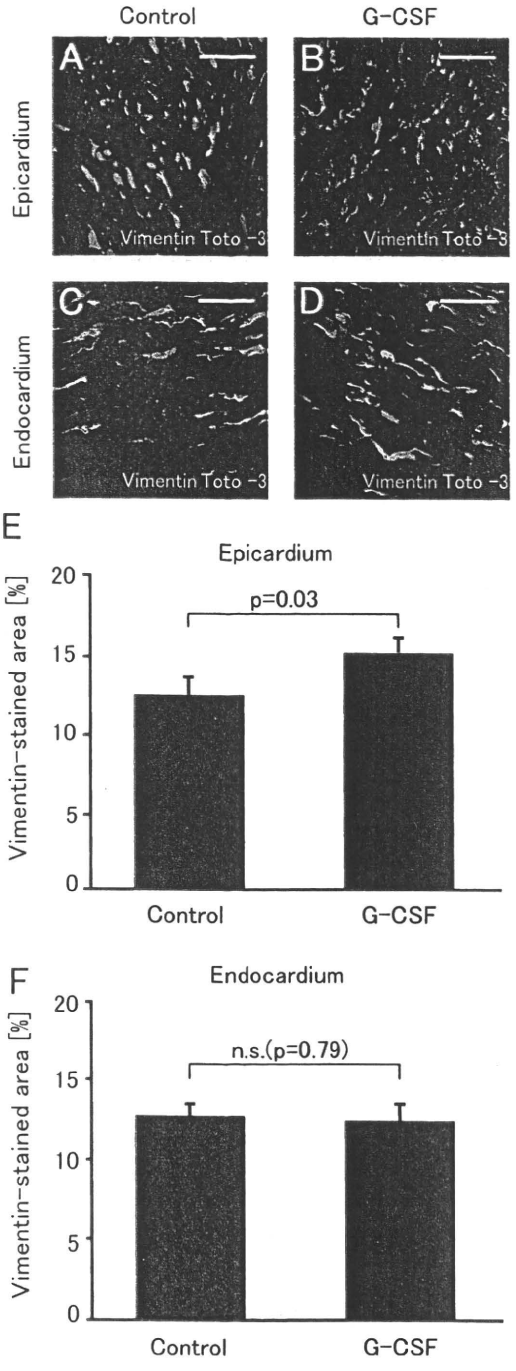

Fig. 8 Immunofluorescent staining for vimentin on the infarcted area

(A)~(D) Representative immunofluorescent microphotograph of the infarcted area using anti-vimentin antibody. (A, B) Comparison of the endocardium between control (A) and G-CSF group (B). (C, D) Comparison of the epicardium between control (C) and G-CSF group (D). Blue = Nuclei stained by TOTO-3. Scale bars show 50μm. (E, F) The vimentin-positive cell density in the endocardium (E) and the epicardium (F). The vimentin-positive cell density of G-CSF group had a tendency to be greater than that of the control group in epicardium, although it was not statistically significant.

clearly expressed α-SMA and vimentin, indicating that they were myofibroblasts. Some also weakly expressed CD45. In the chronic phase of cardiac remodeling, GFP $^{+}$ fibroblast-like cells were still present in the scar tissue of the heart. These cells were positive for vimentin, but most of them were negative for α-SMA. These results indicated that hematopoietic stem cell-derived cells migrated into the infarcted area, and differentiated into myofibroblasts in the acute phase, and became mature fibroblasts by the chronic phase. G-CSF treatment was associated with an increased number of infiltrating myofibroblasts in both groups, as well as a decrease in mortality and an improvement cardiac function in the chronic phase. Moreover, we found that hematopoietic stem cell-derived cells (possibly monocytes) contributed the accumulation of myofibroblasts at the perivascular fibrosis area in pressure overload-induced cardiac hypertrophy model.[21] These results implicate the infiltration of myofibroblasts as critical in the prevention of cardiac remodeling.

The present study showed that G-CSF significantly increased the thickness of the infarcted wall. Moreover, we found that G-CSF significantly increased the cell density of the endothelial cells, α-SMA positive cells and vimentin positive cells but not the cardiomyocytes. However, both α-SMA and vimentin is not a specific marker for special cell types. The α-SMA was expressed in various cell types such as smooth muscle cells, cardiac myofibroblasts, and juvenile cardiomyocytes. Vimentin was mainly expressed in myofibroblasts, but was expressed in other cell types. From the finding of the cell morphology, we supposed that some of α-SMA positive cells might be vascular smooth muscle cells. We also think that most of the cells positive for α-SMA and vimentin might be myofibroblasts, the origin of which might be the mobilized monocytes by G-CSF administration. Taken together, the present findings indicated that G-CSF increased the BM-derived cells in the infarcted area, which may play an important role in modulating post-MI remodeling. This phenomenon was basically in accordance with our previous observation obtained from BM transplanted mice. A number of cell transplantation experiments revealed that fibroblasts, smooth muscle cells, cardiomyocytes and even skeletal muscle cells improved cardiac remodeling and function when they were transplanted into the infarcted area after MI.[6,23-28] The increased cellular density might be critically involved in the healing process of myocardial infarction by secreting extracellular matrix, angiogenic growth factors and cytokines, which may accelerate healing process. Previous papers reported the molecular mechanism of the action of G-CSF.

Recently, Harada reported that G-CSF directly binds to G-CSF receptors on cardiomyocytes, activating the JAK/STAT pathway, and preventing apoptosis in the late

phase after MI. This effect was proposed to improve cardiac remodeling.[29] An anti-apoptotic effect on cardiomyocytes might also play a role in the improvement of cardiac remodeling mediated by G-CSF in our study. In addition, endothelial progenitor cells might also play a role in the regeneration of the infarcted myocardium in the chronic phase. Cardiac progenitor cells have also been shown to be resident in the heart,[30] and we supposed that they also participate in the healing process after MI. These findings indicated that these mechanisms may collaboratively work and improved the cardiac function. A great deal of clinical research up until 2005 involved harvesting mononuclear cells from BM or peripheral blood and infusing them through a catheter into a coronary artery to treat acute myocardial infarction. Strauer and colleagues first reported transplantation of BM mononuclear cells 4.8-13.5 days after a myocardial infarction in 10 acute myocardial infarction patients, which resulted in a slight decrease in left-ventricular end-systolic dimension and infarct region, and an increase in the left-ventricular ejection fraction and regional function.[6] The TOPCARE-AMI trial allocated 20 patients with reperfused acute myocardial infarction to receive intracoronary infusion of either BM-derived or circulating blood-derived progenitor cells into the infarct artery at 4.3±1.5 days. The results from this trial indicated a significant increase in global left ventricular ejection fraction, improved regional wall motion, and reduced end-systolic left ventricular volumes at the 4-month follow-up investigation. At the one year follow-up investigation the transplanted group revealed an increased EF, reduced infarct size, and absence of reactive hypertrophy without significant complication, suggesting functional regeneration of the infarcted ventricles[31-33] (41-43). The BOOST trial, and Fernandes-Aviles and colleagues also transplanted BM mononuclear cells 4.8-13.5 days after a myocardial infarction in acute myocardial infarction patients. In most of the studies, transplantation resulted in similar results.[34,35] The IACT Study transplanted BM mononuclear cells via catheter in patients with chronic MI, and reported that functional and metabolic regeneration of infarcted and chronically avital tissue could be realized.[36]

In conclusion, the precise investigation of molecular mechanisms and the double-blind clinical trial will clarify the usefulness of this cytokine therapy for the prevention of cardiac remodeling after myocardial infarction.

References

1. Orlic D, Kajstura J, Chimenti S, Limana F, Jakoniuk I, Quaini F, Nadal-Ginard B, Bodine DM, Leri A, Anversa P: Mobilized bone marrow cells repair the infarcted heart, improving function and survival. Proc Natl Acad Sci U S A 2001; 98: 10344-10349
2. Norol F, Merlet P, Isnard R, Sebillon P, Bonnet N, Cailliot C, Carrion C, Ribeiro M, Charlotte F, Pradeau P, Mayol J-F, Peinnequin A, Drouet M, Safsafi K, Vernant J-P, Herodin F: Influence of mobilized stem cells on myocardial infarct repair in a nonhuman primate model. Blood 2003; 102: 4361-4368
3. Asahara T, Masuda H, Takahashi T, Kalka C, Pastore C, Silver M, Kearne M, Magner M, Isner JM: Bone Marrow Origin of Endothelial Progenitor Cells Responsible for Postnatal Vasculogenesis in Physiological and Pathological Neovascularization. Circ Res 1999; 85: 221-228
4. Zhang S, Wang D, Estrov Z, Raj S, Willerson JT, Yeh ETH: Both Cell Fusion and Transdifferentiation Account for the Transformation of Human Peripheral Blood CD34-Positive Cells Into Cardiomyocytes *In vivo*. Circulation 2004; 110: 3803-3807
5. Kajstura J, Rota M, Whang B, Cascapera S, Hosoda T, Bearzi C, Nurzynska D, Kasahara H, Zias E, Bonafe M, Nadal-Ginard B, Torella D, Nascimbene A, Quaini F, Urbanek K, Leri A, Anversa P: Bone Marrow Cells Differentiate in Cardiac Cell Lineages After Infarction Independently of Cell Fusion. Circ Res 2005; 96: 127-137
6. Strauer BE, Brehm M, Zeus T, Kostering M, Hernandez A, Sorg RV, Kogler G, Wernet P: Repair of Infarcted Myocardium by Autologous Intracoronary Mononuclear Bone Marrow Cell Transplantation in Humans. Circulation 2002; 106: 1913-1918
7. Weissman IL, Anderson DJ, Gage F: STEM AND PROGENITOR CELLS: Origins, Phenotypes, Lineage Commitments, and Transdifferentiations. Ann Rev Cell Dev Biol 2001; 17: 387-403
8. Richard Poulsom MRA, Stuart J. Forbes, Nicholas A. Wright,: Adult stem cell plasticity. J Pathol 2002; 197: 441-456
9. Badorff C, Brandes RP, Popp R, Rupp S, Urbich C, Aicher A, Fleming I, Busse R, Zeiher AM, Dimmeler S: Transdifferentiation of Blood-Derived Human Adult Endothelial Progenitor Cells Into Functionally Active Cardiomyocytes. Circulation 2003; 107: 1024-1032
10. Orlic D, Kajstura J, Chimenti S, Jakoniuk I, Anderson SM, Li B, Pickel J, McKay R, Nadal-Ginard B, Bodine DM, Leri A, Anversa P: Bone marrow cells regenerate infarcted myocardium. Nature 2001; 410:701-705
11. Jackson KA, Majka SM, Wang H, Pocius J, Hartley CJ, Majesky MW, Entman ML, Michael LH, Hirschi KK, Goodell MA: Regeneration of ischemic cardiac muscle and vascular endothelium by adult stem cells. J Clin Invest 2001; 107: 1395-1402
12. Makino S, Fukuda K, Miyoshi S, Konishi F, Kodama H, Pan J, Sano M, Takahashi T, Hori S, Abe H, Hata J-i, Umezawa A, Ogawa S: Cardiomyocytes can be generated from marrow stromal cells *in vitro*. J Clin Invest 1999; 103: 697-705
13. Hakuno D, Fukuda K, Makino S, Konishi F, Tomita Y, Manabe T, Suzuki Y, Umezawa A, Ogawa S: Bone Marrow-Derived Regenerated Cardiomyocytes (CMG Cells) Express Functional Adrenergic and Muscarinic Receptors. Circulation 2002; 105: 380-386
14. Fukuda K: Development of Regenerative Cardiomyocytes from Mesenchymal Stem Cells for Cardiovascular Tissue Engineering. Artif Organs 2001; 25: 187-193
15. Alvarez-Dolado M, Pardal R, Garcia-Verdugo JM, Fike JR, Lee HO, Pfeffer K, Lois C, Morrison SJ, Alvarez-Buylla A: Fusion of bone-marrow-derived cells with Purkinje neurons, cardiomyocytes and hepatocytes. Nature 2003; 425: 968-973
16. Murry CE, Soonpaa MH, Reinecke H, Nakajima H, Nakajima HO, Rubart M, Pasumarthi KBS, Ismail Virag J, Bartelmez SH, Poppa V, Bradford G, Dowell JD, Williams DA, Field LJ: Haematopoietic stem cells do not transdifferentiate into cardiac myocytes in myocardial infarcts. Nature 2004; 428: 664-668
17. Balsam LB, Wagers AJ, Christensen JL, Kofidis T, Weissman IL, Robbins RC: Haematopoietic stem cells adopt mature haematopoietic fates in ischaemic myocardium. Nature 2004; 428: 668-673
18. Toma C, Pittenger MF, Cahill KS, Byrne BJ, Kessler PD: Human Mesenchymal Stem Cells Differentiate to a Cardiomyocyte Phenotype in the Adult Murine Heart. Circulation 2002; 105: 93-98
19. Tomita S, Li R-K, Weisel RD, Mickle DAG, Kim E-J, Sakai T, Jia

Z-Q. Autologous Transplantation of Bone Marrow Cells Improves Damaged Heart Function. Circulation 1999; 100: II-247-256
20. Kawada H, Fujita J, Kinjo K, Matsuzaki Y, Tsuma M, Miyatake H, Muguruma Y, Tsuboi K, Itabashi Y, Ikeda Y, Ogawa S, Okano H, Hotta T, Ando K, Fukuda K: Nonhematopoietic mesenchymal stem cells can be mobilized and differentiate into cardiomyocytes after myocardial infarction. Blood 2004; 104: 3581-3587
21. Endo J, Sano M, Fujita J, Hayashida K, Yuasa S, Aoyama N, Takehara Y, Kato O, Makino S, Ogawa S, Fukuda K: Bone Marrow Derived Cells Are Involved in the Pathogenesis of Cardiac Hypertrophy in Response to Pressure Overload. Circulation 2007; 116: 1176-1184
22. Fujita J, Mori M, Kawada H, Ieda Y, Tsuma M, Matsuzaki Y, Kawaguchi H, Yagi T, Yuasa S, Endo J, Hotta T, Ogawa S, Okano H, Yozu R, Ando K, Fukuda K: Administration of Granulocyte Colony-Stimulating Factor after Myocardial Infarction Enhances the Recruitment of Hematopoietic Stem Cell-Derived Myofibroblasts and Contributes to Cardiac Repair. Stem Cells 2007 ;25:2750-2759
23. Scorsin M, Hagege A, Vilquin JT, Fiszman M, Marotte F, Samuel JL, Rappaport L, Schwartz K, Menasche P: Comparison of the effects of fetal cardiomyocyte and skeletal myoblast transplantation on postinfarction left ventricular function. J Thorac Cardiovasc Surg 2000; 119: 1169-1175
24. Koh GY, Soonpaa MH, Klug MG, Pride HP, Cooper BJ, Zipes DP, Field LJ: Stable fetal cardiomyocyte grafts in the hearts of dystrophic mice and dogs. J Clin Invest 1995; 96: 2034-2042
25. Jain M, DerSimonian H, Brenner DA, Ngoy S, Teller P, Edge ASB, Zawadzka A, Wetzel K, Sawyer DB, Colucci WS, Apstein CS, Liao R: Cell Therapy Attenuates Deleterious Ventricular Remodeling and Improves Cardiac Performance After Myocardial Infarction. Circulation 2001; 103: 1920-1927
26. Taylor DA, Atkins BZ, Hungspreugs P, Jones TR, Reedy MC, Hutcheson KA, Glower DD, Kraus WE: Regenerating functional myocardium: improved performance after skeletal myoblast transplantation. Nat Med 1998; 4: 929-933
27. Murry CE, Wiseman RW, Schwartz SM, Hauschka SD: Skeletal Myoblast Transplantation for Repair of Myocardial Necrosis. J Clin Invest 1996; 98: 2512-2523
28. Chiu RC, Zibaitis A, Kao RL: Cellular cardiomyoplasty: myocardial regeneration with satellite cell implantation. Ann Thorac Surg 1995; 60: 12-18
29. Harada M, Qin Y, Takano H, Minamino T, Zou Y, Toko H, Ohtsuka M, Matsuura K, Sano M, Nishi J, Iwanaga K, Akazawa H, Kunieda T, Zhu W, Hasegawa H, Kunisada K, Nagai T, Nakaya H, Yamauchi-Takihara K, Komuro I: G-CSF prevents cardiac remodeling after myocardial infarction by activating the Jak-Stat pathway in cardiomyocytes. Nat Med 2005; 11: 305-311
30. Beltrami AP, Urbanek K, Kajstura J, Yan SM, Finato N, Bussani R, Nadal-Ginard B, Silvestri F, Leri A, Beltrami CA, Anversa P: Evidence that human cardiac myocytes divide after myocardial infarction. N Engl J Med 2001; 344: 1750-175
31. Assmus B, Schachinger V, Teupe C, Britten M, Lehmann R, Dobert N, Grunwald F, Aicher A, Urbich C, Martin H, Hoelzer D, Dimmeler S, Zeiher AM: Transplantation of Progenitor Cells and Regeneration Enhancement in Acute Myocardial Infarction (TOPCARE-AMI). Circulation 2002; 106: 3009-3017
32. Schachinger V, Assmus B, Britten MB, Honold J, Lehmann R, Teupe C, Abolmaali ND, Vogl TJ, Hofmann WK, Martin H, Dimmeler S, Zeiher AM: Transplantation of progenitor cells and regeneration enhancement in acute myocardial infarction: final one-year results of the TOPCARE-AMI Trial. J Am Coll Cardiol 2004; 44: 1690-1699
33. Britten MB, Abolmaali ND, Assmus B, Lehmann R, Honold J, Schmitt J, Vogl TJ, Martin H, Schachinger V, Dimmeler S, Zeiher AM: Infarct Remodeling After Intracoronary Progenitor Cell Treatment in Patients With Acute Myocardial Infarction (TOPCARE-AMI): Mechanistic Insights From Serial Contrast-Enhanced Magnetic Resonance Imaging. Circulation 2003; 108: 2212-2218
34. Wollert KC, Meyer GP, Lotz J, Ringes-Lichtenberg S, Lippolt P, Breidenbach C, Fichtner S, Korte T, Hornig B, Messinger D, Arseniev L, Hertenstein B, Ganser A, Drexler H: Intracoronary autologous bone-marrow cell transfer after myocardial infarction: the BOOST randomised controlled clinical trial. Lancet 2004; 364: 141-148
35. Fuchs S, Satler LF, Kornowski R, Okubagzi P, Weisz G, Baffour R, Waksman R, Weissman NJ, Cerqueira M, Leon MB, Epstein SE: Catheter-based autologous bone marrow myocardial injection in no-option patients with advanced coronary artery disease: a feasibility study. J Am Coll Cardiol 2003; 41: 1721-1724
36. Strauer BE, Brehm M, Zeus T, Bartsch T, Schannwell C, Antke C, Sorg RV, Kogler G, Wernet P, Muller HW, Kostering M: Regeneration of human infarcted heart muscle by intracoronary autologous bone marrow cell transplantation in chronic coronary artery disease: the IACT Study. J Am Coll Cardiol 2005; 46: 1651-1658

Biochemical and Biophysical Research Communications 373 (2008) 30–35

Contents lists available at ScienceDirect

Biochemical and Biophysical Research Communications

journal homepage: www.elsevier.com/locate/ybbrc

Inhalation of hydrogen gas reduces infarct size in the rat model of myocardial ischemia–reperfusion injury

Kentaro Hayashida [b], Motoaki Sano [a,d,*], Ikuroh Ohsawa [e,f], Ken Shinmura [c], Kayoko Tamaki [c], Kensuke Kimura [b], Jin Endo [b], Takaharu Katayama [b], Akio Kawamura [b], Shun Kohsaka [b], Shinji Makino [a], Shigeo Ohta [e], Satoshi Ogawa [b], Keiichi Fukuda [a]

[a] Department of Regenerative Medicine and Advanced Cardiac Therapeutics, Keio University School of Medicine, 35 Shinanomachi Shinjuku-ku, Tokyo 160-8582, Japan
[b] Division of Cardiology, Keio University School of Medicine, Tokyo 160-8582, Japan
[c] Division of Geriatric Medicine, Department of Internal Medicine, Keio University School of Medicine, Tokyo 160-8582, Japan
[d] Precursory Research for Embryonic Science and Technology (PRESTO), Japan Science and Technology Agency, Saitama 332-0012, Japan
[e] Department of Biochemistry and Cell Biology, Institute of Development and Aging Science, Graduate School of Medicine, Nippon Medical School, Kawasaki city 211-8533, Japan
[f] Department of Biochemistry and Cell Biology, The Center of Molecular Hydrogen Medicine, Institute of Development and Aging Science, Graduate School of Medicine, Nippon Medical School, Kawasaki city 211-8533, Japan

ARTICLE INFO

Article history:
Received 19 May 2008
Available online 9 June 2008

Keywords:
Ischemia–reperfusion injury
Anti-oxidant
Myocardial infarction
H_2

ABSTRACT

Inhalation of hydrogen (H_2) gas has been demonstrated to limit the infarct volume of brain and liver by reducing ischemia–reperfusion injury in rodents. When translated into clinical practice, this therapy must be most frequently applied in the treatment of patients with acute myocardial infarction, since angioplastic recanalization of infarct-related occluded coronary artery is routinely performed. Therefore, we investigate whether H_2 gas confers cardioprotection against ischemia–reperfusion injury in rats. In isolated perfused hearts, H_2 gas enhances the recovery of left ventricular function following anoxia-reoxygenation. Inhaled H_2 gas is rapidly transported and can reach 'at risk' ischemic myocardium before coronary blood flow of the occluded infarct-related artery is reestablished. Inhalation of H_2 gas at incombustible levels during ischemia and reperfusion reduces infarct size without altering hemodynamic parameters, thereby preventing deleterious left ventricular remodeling. Thus, inhalation of H_2 gas is promising strategy to alleviate ischemia–reperfusion injury coincident with recanalization of coronary artery.

Acute myocardial infarction is a leading cause of death worldwide. Reduction of infarct size is an important therapeutic goal, since the size of the infarct is directly linked to short-term and long-term morbidity and mortality [1]. The prognosis of acute myocardial infarction has been improved dramatically with the development of highly successful approaches to restore blood flow by primary percutaneous coronary intervention (PCI) to the ischemic tissue [2]. Paradoxically, while coronary reperfusion improves the prognosis of acute myocardial infarction, it also leads to myocardial reperfusion injury by extending myocardial damage within the ischemic period [3]. Studies in animal models of acute myocardial infarction show that reperfusion injury accounts for up to 50% of the final size of a myocardial infarct [4]. Therefore, intervention to alleviate reperfusion injury at the time of coronary recanalization has been considered to be the promising strategy to further decrease infarct size and improve the prognosis after myocardial infarction.

The accelerated generation of reactive oxygen species (ROS) by reperfusion of the ischemic myocardium is a potential mediator of reperfusion injury [5–7]. Many attempts have been made to inhibit ROS production to limit the extent of reperfusion injury. However, the administration of ROS scavengers at the time of reperfusion has produced conflicting results [8,9]. That can be partially explained by the dual role of ROS in ischemia-reperfused hearts. The majority of detrimental effects associated with lethal reperfusion injury are attributed to hydroxy radical ($^{\cdot}OH$), the most highly reactive oxygen species. By comparison, superoxide anion radical ($O_2^{-\cdot}$) and hydrogen peroxide (H_2O_2) have less oxidative energy and, paradoxically, are implicated as crucial signaling components in the establishment of favorable tolerance to oxidative stress upon ischemia–reperfusion [10,11]. Consequently, the inhibition of both pathways can be deleterious.

Recently, Ohsawa et al. demonstrated that molecular hydrogen (H_2) is a novel anti-oxidant with certain unique properties. (1) H_2 is permeable to cell membranes and can target organelles,

* Corresponding author. Address: Department of Regenerative Medicine and Advanced Cardiac Therapeutics, Keio University School of Medicine, 35 Shinanomachi Shinjuku-ku, Tokyo 160-8582, Japan. Fax: +81 3 5363 3875.
E-mail address: msano@sc.itc.keio.ac.jp (M. Sano).

0006-291X/$ - see front matter © 2008 Elsevier Inc. All rights reserved.
doi:10.1016/j.bbrc.2008.05.165

including mitochondria and nuclei; (2) H_2 specifically quenches exclusively detrimental ROS, such as ·OH and peroxynitrite ($ONOO^-$), while maintaining the metabolic oxidation–reduction reaction and other less potent ROS, such as $O_2^{-\cdot}$, H_2O_2, and nitric oxide (NO·); (3) inhalation of H_2 gas limits the infarct volume of brain and liver if given at the appropriate time during reperfusion [12,13]. However, clinical application of reperfusion therapy for these organs is limited. When translated into the clinical practice, H_2 gas inhalation therapy must be most frequently applied in the treatment of patients with acute myocardial infarction, since angioplastic recanalization of occluded infarct-related coronary artery is routinely performed.

The aim of this study was to investigate whether inhalation of H_2 gas exerts cardioprotective effects during myocardial ischemia–reperfusion. We showed the inhaled H_2 gas is rapidly transported and can reach even 'at risk' ischemic myocardium before coronary blood flow of the occluded infarct-related artery is reestablished. Inhalation of H_2 gas during ischemia and reperfusion significantly reduces infarct size without altering hemodynamic parameters, thereby preventing deleterious left ventricular (LV) remodeling.

Materials and methods

Animals. All experimental procedures and protocols were approved by the Animal Care and Use Committees of the Keio University and conformed to the NIH Guide for the Care and Use of Laboratory Animals. Eight-week-old male Wistar rats were artificially ventilated under anesthesia with ketamine (60 mg/kg) and xylazine (15 mg/kg) given intraperitoneally. Temperature was maintained at 37.5 ± 0.5 °C using a thermostatically controlled heating blanket connected to a thermometer probe placed in the rectum. H_2 gas was administered through a ventilator and the flow volume was controlled by a gas flowmeter TF-1 (YUTAKA Engineering Corporation, Tokyo, Japan). The concentration of H_2 in the gas mixture was determined using the Breath Gas Analyzer Model TGA-2000 (TERAMECS, Kyoto, Japan). Saturation of arterial oxygen level (SaO_2) was monitored by Clip sensor (PDR-43C) connected to Stand Alone Pulseoxymeter (CANL425SV). A Millar transducer catheter (SPR-320) was placed in the LV cavity via the left internal artery to monitor LV pressure using Polygraph system (NIHON KODEN; PEG-1000).

Myocardial ischemia–reperfusion model. Regional myocardial ischemia was induced by transient occlusion of the left anterior descending coronary artery. After 30 min of ischemia, we removed the tube for myocardial reperfusion and closed the thorax with the suture intact. The suture around the coronary artery was retied 24 h after reperfusion and 2% Evans blue dye was injected into the LV cavity to retrospectively delineate the area at risk of myocardial infarction. The heart was removed, washed in phosphate buffered saline, and then sliced into sequential 1 mm thick sections. We stained the sections with 2,3,5-triphenyltetrazolium chloride (TTC) (3%) then measured the infarct (white), non-infarct (red), non-ischemic, (blue), and at risk areas (AAR) (white and red).

Echocardiography. Rats were anesthetized by inhalation with 1.5% isoflurane. Animals were anchored to a positionable platform in a supine position. Short axis echocardiography was accomplished with a Vevo 660 system (VisualSonics) with the use of a 600 series real-time microvisualization scanhead probe.

Measurement of H_2 gas concentration. H_2 gas concentration was measured in tissues using a needle-type H_2 sensor (Unisense). The electrode current was measured with a picoammeter (Keithley) attached to a strip chart. The negative current obtained from the H_2 sensor was converted to regional H_2 concentration using a calibration curve generated from known levels of H_2 saturated saline.

Langendorff-perfusion of the heart. Hearts were excised quickly from heparinized Wistar male rats (350 g) and perfused with modified Krebs–Henseleit buffer (118 mmol/l NaCl, 25 mmol/l $NaHCO_3$, 4.7 mmol/l KCl, 1.2 mmol/l $MgSO_4$, 1.2 mmol/l KH_2PO_4, 1.75 mmol/l $CaCl_2$, 0.5 mmol/l EDTA, 11 mmol/l glucose, and 5 mmol/l pyruvate) equilibrated with a gas mixture comprised of 95% O_2/5% CO_2 at 37 °C. Coronary perfusion pressure was maintained at 70 mmHg. A plastic catheter with a latex balloon was inserted into the LV. Before the induction of anoxia, hearts were paced at 5 Hz, and the LV end-diastolic pressure was adjusted to 10 mmHg by filling the balloon with water. Pacing was turned off during anoxia and turn on 10, 20, 30, or 40 min after reoxygenation to measure the recovery of LV function. Indices of LV function [LV systolic pressure, LVSP; LV diastolic pressure, LVDP; LV developed pressure (LVDP = LVSP − LVDP); and LV peak positive and negative dP/dt] were recorded as described previously [14–17].

Immunohistochemical procedures. Sample fixation, embedding, sectioning, and blocking were performed as described previously [18]. Briefly, hearts were perfused from the apex with PBS, perfusion-fixed with 4% paraformaldehyde/PBS, dissected, subsequently cryoprotected in sucrose solutions at 4 °C, embedded in OCT compound (Miles Scientific, Naperville, IL), and quickly frozen in liquid nitrogen. The fixed hearts were sectioned (8 μm) using a CM3050S cryostat (Leica, Nussloch, Germany). For immunostaining, sections were blocked in 5% BSA for 30 min at room temperature and stained with anti-8OH-dG (MOG-020P; Japan Institute for the Control of Aging; 1:800) antibodies overnight at 4 °C. Secondary antibodies conjugated Alexa Fluor 546 (Molecular Probes, Eugene, OR, USA; 1:200) were applied for 1 h at 4 °C. Nuclei were stained with TO-PRO-3 (Molecular Probes) in a mounting medium. Slides were observed under Fluorescence Microscope (LYMPUS BX-60). The 8-OHdG positive area as percentage of total left ventricles at serial short axis sections was measured by planimetry using Image/J software from the National Institutes of Health (Bethesda, MD, USA).

Statistical analyses. Values are presented as means ± SEM. Statistical significance was evaluated using the unpaired Student's *t*-tests for comparisons between two mean values. Multiple comparisons between more than three groups were performed using ANOVA. A value of $P < 0.05$ was considered statistically significant.

Results

H_2 gas improves the recovery of left ventricular function during reoxygenation after anoxia in isolated perfused hearts

We first studied the effect of H_2 gas on the functional recovery after anoxia-reoxygenation in Langendorff-perfused rat hearts. Hearts were subjected to 40 min of anoxic perfusion with buffer equilibrated with either 100% N_2 (Control group) or 100% H_2 (H_2 group) followed by 40 min of aerobic reperfusion with buffer equilibrated with 95% O_2 and 5% CO_2 (Fig. 1A). H_2 gas significantly improved the recovery of LV developed pressure (LVDP), positive dP/dt, and negative dP/dt 40 min after reoxygenation ($n = 10$, $^*P < 0.05$, compared to control group, Fig. 1B).

Inhalation of H_2 gas immediately increases the intramyocardial H_2 gas concentration

Before we determined whether inhalation of hydrogen (H_2) gas confers cardioprotection against ischemia–reperfusion injury, the regional delivery of inhaled H_2 gas was investigated by monitoring the time-course of changes in H_2 levels using a needle-shaped

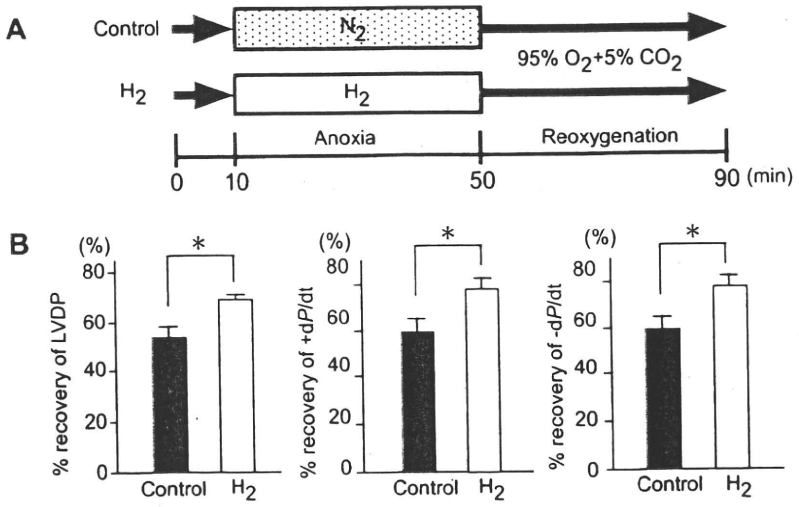

Fig. 1. H_2 gas improves the recovery of left ventricular function during reoxygenation after anoxia in isolated perfused hearts. (A) Experimental protocol of aoxia-reoxygenation. Isolated perfused rat hearts were subjected to 40 min of anoxia with buffer equilibrated with either 100% N_2 (control group) or 100% H_2 (H_2 group) followed by 40 min of aerobic reperfusion. (B) Comparison of percentage recovery of LVDP and peak positive and negative dP/dt 40 min after reoxygenation between control group and H_2 inhalation group (n = 10, $^*P < 0.05$, compared to control group).

hydrogen sensor electrode inserted directly into the tissues. When 2% H_2 gas was inhaled, the arterial H_2 levels started to increase 2 min after inhalation of H_2 gas and reached a maximum level after 5 min [1.82 ± 0.02% (n = 5)]. The incremental rate of H_2 saturation for the non-ischemic myocardium was similar to that observed in arterial blood with attaining a maximum of 1.73 ± 0.02% (n = 5) (Fig. 2A). By contrast, the rate of increase in the H_2 saturation was slower in the center of the thigh muscle with attaining a maximum level of 0.50 ± 0.03% (n = 5) after 30 min (Fig. 2B and Supplementary Fig.).

Of note, H_2 gas levels were increased even in the ischemic myocardium (Fig. 2C). Although the incremental rate of H_2 saturation was slower in the ischemic myocardium than in the non-ischemic myocardium, the peak level of H_2 in the ischemic myocardium was reached at approximately two thirds of the value observed in the non-ischemic myocardium (Fig. 2D). After restoration of coronary artery blood flow, the level of H_2 in the ischemic myocardium immediately increased to the level observed in the non-ischemic myocardium.

Inhalation of H_2 gas protects the heart from ischemia–reperfusion injury

To investigate whether inhalation of H_2 gas protects the heart from ischemia–reperfusion injury, rats were subjected to coronary artery occlusion for 30 min followed by reperfusion for 24 h. H_2 gas was administered at the onset of ischemia and continued for 60 min after reperfusion. H_2 gas has no adverse effect on heart rate and arterial oxygenation (Fig. 3A). There was no significant difference in the temporal profile of LV end-systolic

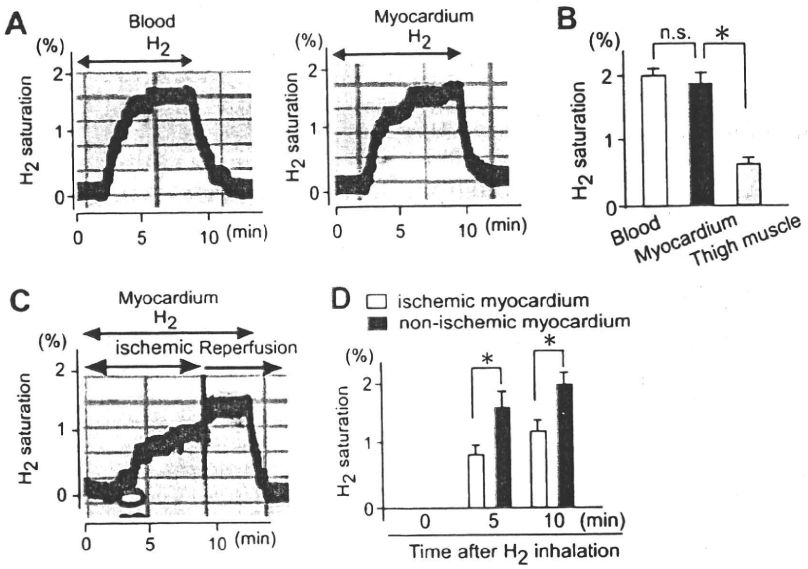

Fig. 2. Inhalation of H_2 gas increases the intramyocardial H_2 gas concentration. H_2 gas at 2% was administered by respiration to intubated rats receiving mechanical ventilation and the concentration of H_2 in tissue was recorded continuously. (A) A needle-type H_2 sensor was inserted in LV cavity (arterial blood) and non-ischemic LV myocardium. (B) Comparison of peak H_2 gas levels between arterial blood, non-ischemic LV myocardium, and thigh muscle (n = 5, $^*P < 0.05$, compared to the level of arterial blood). (C) The changes in the concentration of H_2 in 'at risk' area for infarction during ischemia and reperfusion. (D) Comparison of change in the H_2 concentration between non-ischemic and ischemic myocardium after H_2 inhalation (n = 5, $^*P < 0.05$, compared to the level of non-ischemic myocardium).

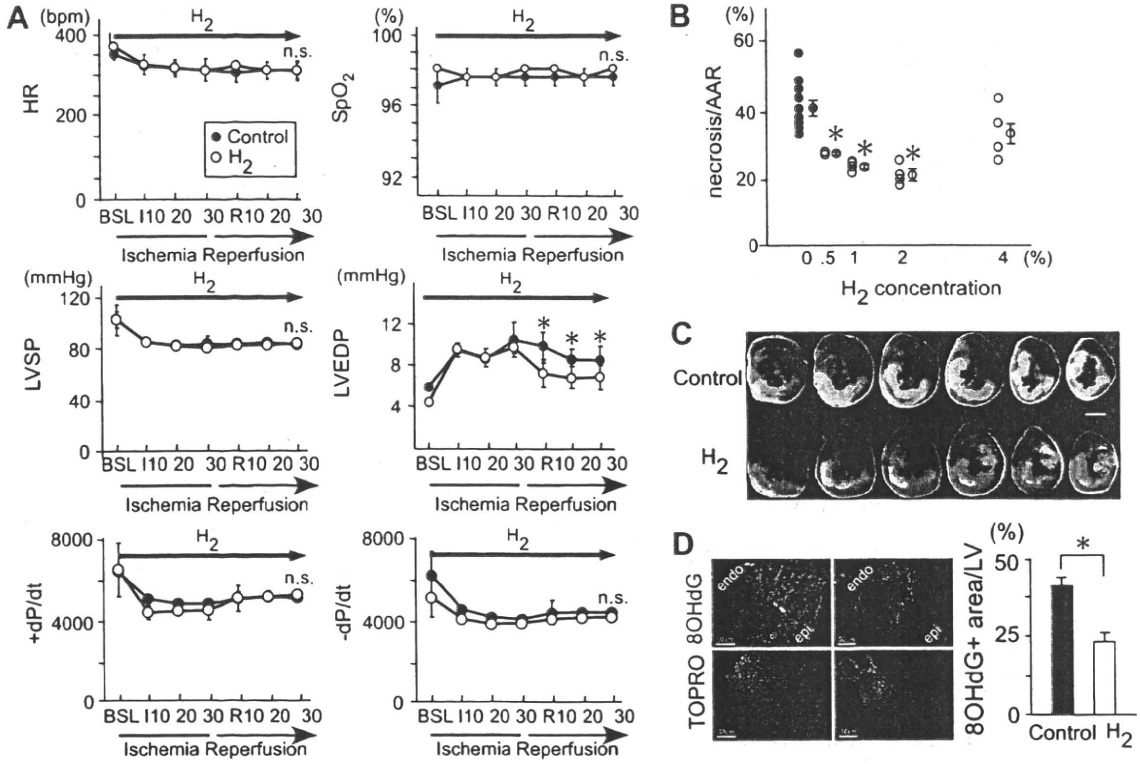

Fig. 3. Inhalation of H_2 reduces infarct size induced by ischemia–reperfusion injury. (A) Changes in heat rate (HR), oxygen saturation by pulse oximetry (SpO_2), and LV systolic pressure (LVSP), LV diastolic pressure (LVEDP) and LV peak positive and negative d*P*/d*t* were monitored during ischemia–reperfusion injury ($n = 5$ in each group). (B) H_2-dependent decrease in infarct size is expressed as the ratio of total infarct area/AAR ($^*P < 0.05$, compared to control group). (C) Representative photographs of serial heart sections obtained from rats subjected to myocardial ischemia–reperfusion injury in the presence or absence of H_2 inhalation. Bar = 2 mm. (D) Immunohistochemical staining with antibodies against 8-OHdG was performed 24 h after ischemia–reperfusion injury. Quantification of 8-OHdG immunoreactive area was expressed as percentage of total LV area at serial short axis sections ($n = 5$, $^*P < 0.05$, H_2 inhalation group compared to control group). endo, endocardium; epi, epicardium.

pressure, LV peak positive and negative LV d*P*/d*t*, between the control group and the 2% H_2 gas inhalation group. Notably, LV-end-diastolic pressure after reperfusion was significantly lower in H_2 gas inhalation group compared to control group ($n = 5$, $^*P < 0.05$).

In the absence of H_2 gas inhalation, infarct size following ischemia–reperfusion was 41.6 ± 2.5% of the area at risk ($n = 9$). By comparison, inhalation of 0.5–2% H_2 gas significantly reduced infarct size, with 2% H_2 gas providing the most prominent effects (21.2 ± 1.6% of area at risk, $n = 4$, Fig. 3B and C). There was no significant difference in area at risk/LV among control group and H_2 gas inhalation groups (data not shown). Consistent with those observations, the quantitative determination of 8-hydroxydeoxyguanosine (8-OHdG) immunoreactive area, a biomarker of oxidative stress, revealed that the level of oxidative injury elicited in the 'at risk' area was significantly smaller in the group receiving 2% H_2 gas inhalation than that of control group ($n = 5$, $^*P < 0.05$, Fig. 3D).

Inhalation of H_2 gas reduces LV remodeling after ischemia–reperfusion injury

To determine the impact of H_2 inhalation at the time of ischemia–reperfusion on pathological LV remodeling, LV morphology and function were monitored by echocardiography 30 days after myocardial ischemia–reperfusion injury. Control rats showed maladaptive pathological remodeling after myocardial infarction, including dilatation of LV cavity, reduced LV systolic function. Notably, inhalation of H_2 gas during myocardial ischemia–reperfusion reduced pathological remodeling after myocardial infarction (Fig. 4).

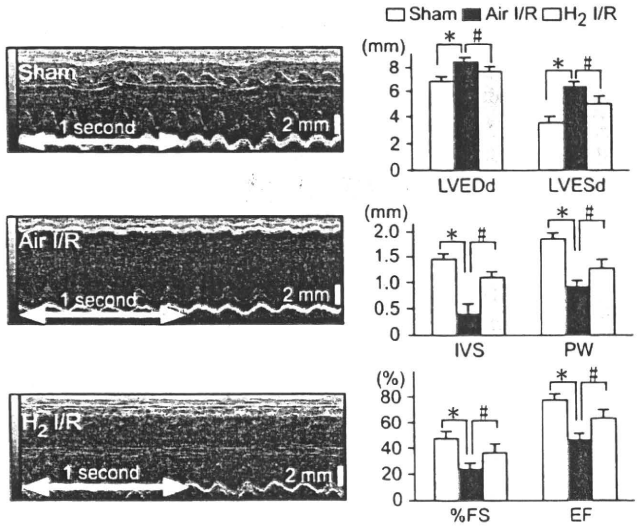

Fig. 4. Inhalation of H_2 gas reduces adverse LV remodeling. Representative M-mode echocardiographic images of sham-operated (sham), ischemia–reperfusion with air inhalation (Air_I/R), and ischemia–reperfusion with H_2 inhalation (H_2_I/R). Measurement of M-mode echocardiographic images in each group. LVEDd, LV endodiastolic diameter (μm); LVESd, LV endosystolic diameter (μm); IVC, intraventricular septum diameter (μm); PW, posterior wall thickness (μm); FS, fractional shortening (%); EF, ejection fraction (%) ($n = 5$, $^*P < 0.05$, compared to sham-operated group; $^\#P < 0.05$, compared to Air_I/R group).

Discussion

This is the first study to demonstrate that inhalation of H_2 gas, at an incombustible level, limit the extent of myocardial infarction

resulting from myocardial ischemia–reperfusion injury, and thereby preserve LV function *in vivo*. The cardioprotective effect of H_2 gas was also confirmed *ex vivo* Langendorff-perfused hearts subjected to anoxia-reoxygenation injury. The anti-oxidant properties of H_2 were confirmed by the demonstration that (1) H_2 improves the recovery of LV function during reoxygenation after anoxia, one of the oxidative stress model, in isolated perfused hearts; (2) inhalation of H_2 gas ameliorates the level of 8-OHdG immunoreactivity in the 'at risk' area for infarction. The anti-oxidant action of molecular H_2 may be explained, at least partially, by direct ROS scavenging effect. However, it remains unclear if the anti-oxidant action of H_2 is also ascribed to the activation of the reperfusion injury salvage kinase pathways or a direct effect on mitochondrial energetics.

Gas inhalation as disease therapy has received recent interest. There are three endogenous gas signaling molecules, known as gasotransmitters, include nitric oxide (NO), carbon monoxide (CO), and hydrogen sulfate (H_2S). The increased production of these gases under stress conditions may reflect the active involvement of these gases in the protective response. In pre-clinical experimental models of disease, including ischemia–reperfusion injury, the inhalation of exogenous CO or H_2S has produced a favorable outcome for most vital organs [19–22]. However, the inherent toxicity of these gases must be investigated for gas inhalation to be considered an effective therapeutic strategy. It is unknown if the therapeutically effective threshold for CO or H_2S can be attained locally in target organs without delivering a potentially toxic level of the gasses via the lungs.

H_2 is not produced endogenously in mammalian cells since the hydrogenase activity responsible for the formation of H_2 gas has not been identified [23]. The spontaneous production of H_2 gas in the human body occurs via fermentation of undigested carbohydrates by resident enterobacterial flora. H_2 is transferred to the portal circulation and excreted through the breath in significant amounts. We demonstrated that inhaled H_2 at therapeutic dose has no adverse effects on the saturation level of arterial oxygen (SpO_2) or hemodynamic parameters, including heart rate and LV pressure. H_2 dissolved in the blood is distributed to tissues proportional to regional blood flow, and is rapidly eliminated by the lungs. Accordingly, the H_2 gas clearance method was employed to measure local blood flow in various tissues [24]. Since the heart is one of the most highly perfused tissues, the intramyocardial H_2 concentration increases immediately following inhalation of H_2, and attaining to almost compatible levels of that observed in arterial blood within 10 min. Of note, the regional H_2 concentration in the ischemic myocardium reaches at two thirds of the value observed in the non-ischemic myocardium. This may occur through gaseous diffusion from the blood in the ventricular cavity and/or adjacent non-ischemic myocardium. These findings indicate that administration of H_2 gas by inhalation, in patients with totally coronary artery occlusion, can efficiently increase the regional concentration of H_2 in the 'at risk' area for myocardial infarction before reestablishing coronary blood flow within the occluded infarct-related artery.

We demonstrated that inhalation of H_2 gas is promising strategies to alleviate ischemia–reperfusion injury at the time of recanalization of coronary artery. When translated into the clinical practice, inhalation of H_2 gas must be most frequently applied in the treatment of patients with acute myocardial infarction in conjunction with routinely performed PCI procedures. Further understanding of the mechanisms underlying the signaling pathways involved in H_2-mediated anti-oxidant activity, and the capacity of H_2 to influence cellular metabolism, is required to fully exploit inhalation of H_2 gas as a therapeutic strategy.

Acknowledgments

We thank M. Okada (NIHON KODEN), S. Kotouda (LMS laboratory and Medical Supplies), C. Ogawa, K. Nishimaki, M. Kamimura, M. Abe, Y. Miyake, H. Kawaguchi, H. Shiozawa, and M. Ono for their technical assistance. M. Sano is a core member of the Global Center-of-Excellence (GCOE) for Human Metabolomics Systems Biology from MEXT. This work was supported by a PRESTO (Metabolism and Cellular Function) grant from the Japanese Science and Technology Agency awarded to M. Sano.

Appendix A. Supplementary data

Supplementary data associated with this article can be found, in the online version, at doi:10.1016/j.bbrc.2008.05.165.

References

[1] A. Volpi, C. De Vita, M.G. Franzosi, E. Geraci, A.P. Maggioni, F. Mauri, E. Negri, E. Santoro, L. Tavazzi, G. Tognoni, Determinants of 6-month mortality in survivors of myocardial infarction after thrombolysis. Results of the GISSI-2 data base. The Ad hoc Working Group of the Gruppo Italiano per lo Studio della Sopravvivenza nell'Infarto Miocardico (GISSI)-2 Data Base, Circulation 88 (1993) 416–429.
[2] E.C. Keeley, J.A. Boura, C.L. Grines, Primary angioplasty versus intravenous thrombolytic therapy for acute myocardial infarction: a quantitative review of 23 randomised trials, Lancet 361 (2003) 13–20.
[3] E. Braunwald, R.A. Kloner, Myocardial reperfusion: a double-edged sword?, J Clin. Invest. 76 (1985) 1713–1719.
[4] D.M. Yellon, D.J. Hausenloy, Myocardial reperfusion injury, N. Engl. J. Med. 357 (2007) 1121–1135.
[5] J.L. Zweier, Measurement of superoxide-derived free radicals in the reperfused heart. Evidence for a free radical mechanism of reperfusion injury, J. Biol. Chem. 263 (1988) 1353–1357.
[6] R. Bolli, B.S. Patel, M.O. Jeroudi, E.K. Lai, P.B. McCay, Demonstration of free radical generation in "stunned" myocardium of intact dogs with the use of the spin trap alpha-phenyl *N-tert*-butyl nitrone, J. Clin. Invest. 82 (1988) 476–485.
[7] T. Vanden Hoek, L.B. Becker, Z.H. Shao, C.Q. Li, P.T. Schumacker, Preconditioning in cardiomyocytes protects by attenuating oxidant stress at reperfusion, Circ. Res. 86 (2000) 541–548.
[8] J.T. Flaherty, B. Pitt, J.W. Gruber, R.R. Heuser, D.A. Rothbaum, L.R. Burwell, B.S. George, D.J. Kereiakes, D. Deitchman, N. Gustafson, et al., Recombinant human superoxide dismutase (h-SOD) fails to improve recovery of ventricular function in patients undergoing coronary angioplasty for acute myocardial infarction, Circulation 89 (1994) 1982–1991.
[9] V.J. Richard, C.E. Murry, R.B. Jennings, K.A. Reimer, Therapy to reduce free radicals during early reperfusion does not limit the size of myocardial infarcts caused by 90 minutes of ischemia in dogs, Circulation 78 (1988) 473–480.
[10] C. Penna, R. Rastaldo, D. Mancardi, S. Raimondo, S. Cappello, D. Gattullo, G. Losano, P. Pagliaro, Post-conditioning induced cardioprotection requires signaling through a redox-sensitive mechanism, mitochondrial ATP-sensitive K^+ channel and protein kinase C activation, Basic Res. Cardiol. 101 (2006) 180–189.
[11] J.M. Downey, M.V. Cohen, A really radical observation—a comment on Penna et al., Basic Res. Cardiol. 101 (2006) 190–191.
[12] I. Ohsawa, M. Ishikawa, K. Takahashi, M. Watanabe, K. Nishimaki, K. Yamagata, K. Katsura, Y. Katayama, S. Asoh, S. Ohta, Hydrogen acts as a therapeutic antioxidant by selectively reducing cytotoxic oxygen radicals, Nat. Med. 13 (2007) 688–694.
[13] K. Fukuda, S. Asoh, M. Ishikawa, Y. Yamamoto, I. Ohsawa, S. Ohta, Inhalation of hydrogen gas suppresses hepatic injury caused by ischemia/reperfusion through reducing oxidative stress, Biochem. Biophys. Res. Commun. 361 (2007) 670–674.
[14] M. Tani, Y. Suganuma, H. Hasegawa, K. Shinmura, Y. Hayashi, X. Guo, Y. Nakamura, Changes in ischemic tolerance and effects of ischemic preconditioning in middle-aged rat hearts, Circulation 95 (1997) 2559–2566.
[15] K. Shinmura, K. Tamaki, R. Bolli, Short-term caloric restriction improves ischemic tolerance independent of opening of ATP-sensitive K^+ channels in both young and aged hearts, J. Mol. Cell. Cardiol. 39 (2005) 285–296.
[16] K. Shinmura, K. Tamaki, K. Saito, Y. Nakano, T. Tobe, R. Bolli, Cardioprotective effects of short-term caloric restriction are mediated by adiponectin via activation of AMP-activated protein kinase, Circulation 116 (2007) 2809–2817.
[17] J.P. Headrick, Aging impairs functional, metabolic and ionic recovery from ischemia–reperfusion and hypoxia-reoxygenation, J. Mol. Cell. Cardiol. 30 (1998) 1415–1430.
[18] J. Endo, M. Sano, J. Fujita, K. Hayashida, S. Yuasa, N. Aoyama, Y. Takehara, O. Kato, S. Makino, S. Ogawa, K. Fukuda, Bone marrow derived cells are involved in the pathogenesis of cardiac hypertrophy in response to pressure overload, Circulation 116 (2007) 1176–1184.

[19] C. Szabo, Hydrogen sulphide and its therapeutic potential, Nat. Rev. Drug Discov. 6 (2007) 917–935.
[20] J.W. Elrod, J.W. Calvert, J. Morrison, J.E. Doeller, D.W. Kraus, L. Tao, X. Jiao, R. Scalia, L. Kiss, C. Szabo, H. Kimura, C.W. Chow, D.J. Lefer, Hydrogen sulfide attenuates myocardial ischemia-reperfusion injury by preservation of mitochondrial function, Proc. Natl. Acad. Sci. USA 104 (2007) 15560–15565.
[21] R. Foresti, M.G. Bani-Hani, R. Motterlini, Use of carbon monoxide as a therapeutic agent: promises and challenges, Intensive Care Med. (2008).
[22] A. Kobayashi, K. Ishikawa, H. Matsumoto, S. Kimura, Y. Kamiyama, Y. Maruyama, Synergetic antioxidant and vasodilatory action of carbon monoxide in angiotensin II-induced cardiac hypertrophy, Hypertension 50 (2007) 1040–1048.
[23] M.W. Adams, L.E. Mortenson, J.S. Chen, Hydrogenase, Biochim. Biophys. Acta 594 (1980) 105–176.
[24] K. Aukland, B.F. Bower, R.W. Berliner, Measurement of local blood flow with hydrogen gas, Circ. Res. 14 (1964) 164–187.

IJCA-11113; No of Pages 2

ELSEVIER

International Journal of Cardiology xx (2008) xxx – xxx

International Journal of Cardiology

www.elsevier.com/locate/ijcard

Letter to the Editor

Is mitral regurgitant jet offensive rather than protective for left atrial thrombus?

Kensuke Kimura [a,b,d,*], Kunihiro Suzuki [c,d], Yohei Ohno [a,d], Shigetaka Noma [d], Keiichi Fukuda [a]

[a] *Department of Regenerative Medicine and Advanced Cardiac Therapeutics, Keio University School of Medicine, 35 Shinanomachi, Shinjuku-ku, Tokyo 160-8582, Japan*

[b] *Bridgestone Laboratory of Developmental and Regenerative Neurobiology, Keio University School of Medicine, 35 Shinanomachi, Shinjuku-ku, Tokyo 160-8582, Japan*

[c] *Department of Endocrinology and Metabolism, Dokkyo University School of Medicine, 880 Kitakobayashi, Mibu-cho, Shimotsuga-gun, Tochigi 321-0293, Japan*

[d] *Department of Cardiology, Saiseikai Utsunomiya Hospital, 911-1 Takebayashi-machi, Utsunomiya, Tochigi, 321-0974, Japan*

Received 21 March 2008; accepted 1 June 2008

Keywords: Left atrial thrombus; Mitral regurgitant jet; Atrial fibrillation; Malignancy; Anticoagulant therapy

A 77-year-old man with chronic atrial fibrillation (AF) was admitted to our hospital for dysarthria. Diffusion magnetic resonance imaging showed multiple high signals in the brain, indicating acute emboli. Trans-esophageal echocardiography revealed a giant thrombus in the left atrial (LA) roof with mobile process on its surface. Surprisingly, it was also observed that the surface of thrombus was encroached on by mitral regurgitant (MR) jet (Fig. 1). No pericardial effusion and extra cardiac mass were observed. No remarkable coagulation factor abnormality was detected. Open chest thrombectomy concomitant with simple isolation of pulmonary vein (PV) orifices for AF was successfully performed to prevent a recurrence of lethal emboli. The pathological examination revealed no other contents like cancer cells in the extracted thrombus. He recovered uneventfully after the operation and not only thrombus but also AF disappeared. Oral anticoagulation was started, and then he was discharged. Two months after discharge, he was re-admitted for consciousness disturbance due to hypercalcemia (12.9 mg/dl, corrected). Computed tomography, tumor markers (SCC 3.1 ng/ml, PTH-rp 7.1 pmol/ml) and trans-bronchial lung biopsy indicated that he had a squamous cell carcinoma in the left lower lung lobe. No obvious direct cardiac invasion of carcinoma was documented. Although warfarin was effected (PT-INR 3.4) and moderate MR jet was blown under the recurrence of AF, a giant thrombus reappeared in the LA roof (Fig. 2). No other systemic thrombus was detected except for the LA. Because of metastasis, he was taken the best supportive therapy, and the thrombus was slowly progressive in the LA until he died.

AF is a familiar arrhythmia and is an independent risk factor for emboli. Oral anticoagulation markedly decreases the risk of emboli in patients with AF [1]. It was also reported that the presence of significant MR correlates with a lower incidence of emboli [2]. On the other hand, strong clinical evidence is accumulating on the hypercoagulability of cancer patients [3].

Although we couldn't clearly explain why the thrombus reappeared on the same place, we could speculate that the thrombus was mainly formed at the PV because the concentration of thrombophilic products from lung cancer

* Corresponding author. Bridgestone Laboratory of Developmental and Regenerative Neurobiology, Keio University School of Medicine, 35 Shinanomachi, Shinjuku-ku, Tokyo 160-8582, Japan. Tel.: +81 3 5363 3874; fax: +81 3 5363 3875.

E-mail address: kimuken@cpnet.med.keio.ac.jp (K. Kimura).

0167-5273/$ - see front matter
doi:10.1016/j.ijcard.2008.06.050

Please cite this article as: Kimura K, et al, Is mitral regurgitant jet offensive rather than protective for left atrial thrombus? Int J Cardiol (2008), doi:10.1016/j.ijcard.2008.06.050

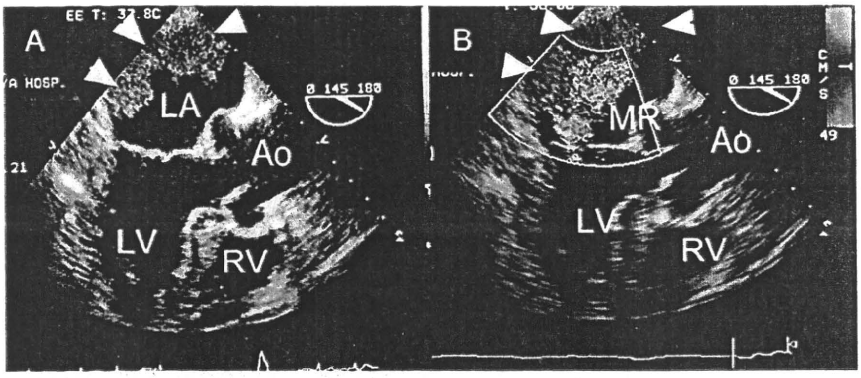

Fig. 1. Trans-esophageal echocardiograms showing a giant thrombus (arrow heads) in the left atrium at the first admission. (A) Moderate mitral regurgitant jet blowing and encroaching on the surface of the thrombus. (B) LV indicates left ventricle; RV, right ventricle; LA, left atrium; Ao, aorta.

cells are higher at the PV, where the blood flow was reduced due to AF. To our knowledge, this is the first description about a recurrent LA giant thrombus regardless of MR jet and anticoagulant therapy in a 77-year-old man with AF. Clinicians should note the potentially offensiveness of MR jet in the AF patients with malignancy, which could overcome to form a thrombus against all defenses.

References

[1] Laupacis A, Albers G, Dalen J, Dunn MI, Jacobson AK, Singer DE. Antithrombotic therapy in atrial fibrillation. Chest 1998;114:579–89.
[2] Wanishsawad C, Weathers LB, Puavilai W. Mitral regurgitation and left atrial thrombus in rheumatic mitral valve disease. A clinicopathologic study. Chest 1995;108:677–81.
[3] Donati MB, Falanga A. Pathogenetic mechanisms of thrombosis in malignancy. Acta Haematol 2001;106:18–24.

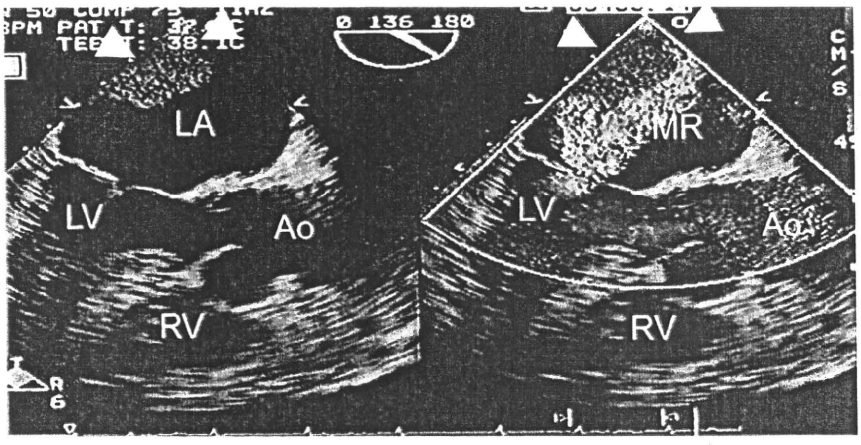

Fig. 2. Trans-esophageal echocardiograms showing a recurrent giant thrombus (arrow heads) in the left atrium at the second admission regardless of severe mitral regurgitant jet. MR indicates mitral regurgitation.

Please cite this article as: Kimura K, et al. Is mitral regurgitant jet offensive rather than protective for left atrial thrombus? Int J Cardiol (2008), doi:10.1016/j.ijcard.2008.06.050

Regulation of Cardiac Nerves: A New Paradigm in The Management of Sudden Cardiac Death?

Masaki Ieda, Kensuke Kimura, Hideaki Kanazawa and Keiichi Fukuda*

Department of Regenerative Medicine and Advanced Cardiac Therapeutics, Keio University School of Medicine, 35 Shinanomachi, Shinjuku-ku, Tokyo 160-8582; Japan

Abstract: The heart is extensively innervated, and its performance is tightly regulated by the autonomic nervous system. To maintain cardiac function, innervation density is stringently controlled, being high in the subepicardium and the central conduction system. In diseased hearts, cardiac innervation density varies, which in turn leads to sudden cardiac death. After myocardial infarction, sympathetic denervation is followed by reinnervation within the heart, leading to unbalanced neural activation and lethal arrhythmia. Diabetic sensory neuropathy causes silent myocardial ischemia, characterized by loss of pain perception during myocardial ischemia, which is a major cause of sudden cardiac death in diabetes mellitus (DM). Despite its clinical importance, the molecular mechanism underlying innervation density remains poorly understood.

We found that cardiac sympathetic innervation is determined by the balance between neural chemoattraction and chemorepulsion, both of which occur in the heart. Nerve growth factor (NGF), which is a potent chemoattractant, is synthesized abundantly by cardiomyocytes and is induced by endothelin-1 upregulation in the heart. In contrast, Sema3a, which is a neural chemorepellent, is expressed strongly in the trabecular layer in early stage embryos and at a lower level after birth, leading to epicardial-to-endocardial transmural sympathetic innervation patterning. We also found that cardiac NGF downregulation is a cause of diabetic neuropathy, and that NGF supplementation rescues silent myocardial ischemia in DM. Both Sema3a-deficient and Sema3a-overexpressing mice showed sudden death or lethal arrhythmias due to disruption of innervation patterning. The present review focuses on the regulatory mechanisms involved in neural development in the heart and their critical roles in cardiac performance.

Keywords: Heart, cardiac nerve, nerve growth factor, Sema3a, arrhythmia, sudden cardiac death.

INTRODUCTION

Cardiac tissues are extensively innervated by autonomic nerves. The sympathetic nervous system produces norepinephrine and increases the heart rate, conduction velocity, as well as myocardial contraction and relaxation. It is well known that sympathetic innervation density, which is high in the subepicardium and the central conduction system, is determined stringently within the heart [1-4]. The regional difference in sympathetic innervation influences cardiac functions to different extents, effectively controlling the heart rate and myocardial contraction and relaxation. Despite its importance, little is known about the developmental and regulatory mechanisms underlying cardiac sympathetic innervation patterning. Moreover, to date there has been no experimental demonstration of the consequences of disrupting this patterning.

Cardiac innervation density is altered in diseased hearts, as in cases of congestive heart failure and myocardial infarction [5-7]. Following myocardial injury, cardiac nerves undergo Wallerian degeneration, which may be followed by neurilemmal cell proliferation and axonal regeneration, resulting in heterogeneous innervation [8, 9]. Unbalanced sympathetic innervation may trigger lethal arrhythmia through ion channel modulation in cardiomyocytes [7, 10, 11]. On the other hand, as the sensory nervous system is responsible for pain perception, cardiac sensory denervation may cause silent myocardial ischemia, characterized by loss of pain perception during myocardial ischemia and frequently leading to sudden cardiac death (SCD) in diabetes mellitus (DM) patients [12]. Despite the severity of these complications, the molecular mechanism that determines innervation density in pathological hearts is poorly understood. Addressing these questions requires a better understanding of the anatomical distribution of cardiac nerves and the molecular mechanism that regulates innervation during development.

In this article, we review the regulatory mechanisms involved in neural development in the heart, as well as its critical roles in cardiac performance.

*Address correspondence to this author at the Department of Regenerative Medicine and Advanced Cardiac Therapeutics, Keio University School of Medicine, 35 Shinanomachi, Shinjuku-ku, Tokyo 160-8582, Japan; Tel: +81-3-5363-3874; Fax: +81-3-5363-3875; E-mail: kfukuda@sc.itc.keio.ac.jp

0929-8673/08 $55.00+.00

CARDIAC NERVE DEVELOPMENT

Neural crest cells migrate and form sympathetic ganglia by mid-gestation, and subsequently proliferate and differentiate into mature neurons [13, 14]. The cardiac sympathetic nerves extend from the sympathetic neurons in stellate ganglia, which are located bilateral to the vertebra. Sympathetic nerve fibers project from the base of the heart into the myocardium, and are located predominantly in the subepicardium of the ventricle [1, 2]. The central conduction system, which includes the sinoatrial node, atrioventricular node, and His bundle, is abundantly innervated compared with the working myocardium [2, 4, 15, 16]. We and others have reported that this regional difference in cardiac sympathetic innervation (innervation patterning) is highly conserved among mammals [2, 4, 17].

The cardiac nervous system also involves afferent nerves. The sensory signals generated in the heart are conducted through cardiac afferent nerves, primarily thinly myelinated Aδ-fibers and nonmyelinated C-fibers [18, 19]. The sensory nerve fibers project to the upper thoracic dorsal horn *via* dorsal root ganglia neurons, which are also derived from neural crest cells [18, 19].

One of the difficulties in analyzing cardiac innervation of the heart has been the lack of suitable molecular markers. However, recent advancements in immunohistochemical techniques have allowed us to stain autonomic nerves using antibodies against nerve-specific markers, such as tyrosine hydroxylase (TH; a sympathetic marker), calcitonin gene-related peptide (CGRP; a sensory marker), protein gene product 9.5 (PGP 9.5; a general peripheral nerve marker), and growth associated protein 43 (GAP43; a nerve sprouting marker). As discussed below, using these specific neural markers, we and others have recently demonstrated that cardiac innervation is strictly organized in the heart during development, whereas in diseased hearts, innervation density appears to be altered dynamically [5, 9, 20-22].

NERVE SPROUTING AND SUDDEN CARDIAC DEATH

It is well known that sympathetic stimulation is important in the generation of SCD in diseased hearts. There is a circadian variation of the frequency of SCD in parallel with sympathetic activity. β-

Blocker therapy prevents SCD secondary to ventricular tachyarrhythmia in ischemic heart disease or congestive heart failure [23, 24]. Immunohistochemical analysis of cardiac nerves in explanted hearts of transplant recipients has revealed a positive correlation between nerve density and clinical history of ventricular tachyarrhythmia [7]. Zhou *et al.* [25] have shown that nerve growth factor (NGF), which is critical for sympathetic nerve sprouting, is upregulated after myocardial infarction (MI) in animal models, resulting in the regeneration of cardiac sympathetic nerves and heterogeneous innervation. In other experiments, it has been shown that augmented myocardial nerve sprouting through NGF infusion after MI results in a dramatic increase in SCD and a high incidence of ventricular tachyarrhythmia, as compared with animals not receiving NGF infusion [5]. These results demonstrate that NGF upregulation and nerve sprouting in diseased hearts may cause lethal arrhythmia and SCD. Despite its importance, the molecular mechanisms that regulate NGF expression and sympathetic innervation in the heart are poorly understood.

THE ENDOTHELIN-1/NGF PATHWAY IS CRITICAL FOR CARDIAC SYMPATHETIC INNERVATION

In general, the growth-cone behavior of nerves is modulated by coincident signaling modulated by neural chemoattractants and chemorepellents synthesized in the innervated tissue. NGF, which is a potent neural chemoattractant, is a prototypic member of the neurotrophin family, the members of which are critical for the differentiation, survival, and synaptic activity of the peripheral sympathetic and sensory nervous systems [26-28]. The levels of NGF expression within innervated tissues correspond approximately to the levels of innervation density [29]. NGF expression increases during development and is altered in diseased hearts [5-7, 30]. In spite of the importance of NGF in neural development, the upstream molecules that regulate NGF expression *in vivo* remained undetermined [31].

Endothelin-1 (ET-1) is a critical factor in the pathogenesis of cardiac hypertrophy, hypertension, and atherosclerosis [32, 33]. Gene targeting of ET-1 and its receptor ET_A has resulted in unexpected craniofacial and cardiovascular abnormalities that have not been observed in other hypertrophic factor-deficient mice [34-37]. These phenotypes are consistent with interference of neural crest differentiation. However, the influence of ET-1 on neural crest development remains to be determined. Therefore, we hypothesized that ET-1 might affect the induction of neurotrophic factors, and that its disruption might contribute to the immature development of neural crest-derived cells [20].

We found that ET-1 (among several hypertrophic factors tested) specifically upregulated NGF expression in primary cultured cardiomyocytes. ET-1-induced NGF augmentation was not observed in cardiac fibroblasts, and this phenomenon was cell type-specific in cardiomyocytes. We also identified the signaling molecules involved in the ET-1/NGF pathway [38]. To study the effects of the ET-1/NGF pathway on the development of the cardiac sympathetic nervous system, we analyzed various gene-modified mouse models. NGF expression, cardiac sympathetic innervation (Fig. **1**), and norepinephrine concentration were reduced in ET-1-deficient mouse (*Edn1*$^{-/-}$) hearts, but not in the hearts of angiotensinogen-deficient mice (*Atg*$^{-/-}$). In *Edn1*$^{-/-}$ mice, the sympathetic stellate ganglia exhibited excessive apoptosis and displayed loss of neurons at the late embryonic stage [14]. Moreover, we have demonstrated that cardiac-specific overexpression of NGF in *Edn1*$^{-/-}$ mice overcomes sympathetic nerve retardation [39]. These findings indicate that ET-1 is a key regulator of NGF expression in cardiomyocytes, and that the ET-1/NGF pathway is critical for sympathetic innervation in the heart [20].

We have previously investigated whether the ET-1/NGF pathway plays a role in sympathetic innervation in diseased hearts [40]. We produced right ventricular hypertrophy in rats by monocrotaline treatment, and analyzed the levels of NGF expression and newly developed sympathetic nerves in the hearts [41, 42]. The levels of ET-1, NGF, and brain natriuretic peptide (hypertrophy marker) expression were strongly increased in the right ventricles in monocrotaline-treated rats [43-45]. Sympathetic nerves that were immunopositive for polysialylated neural cell adhesion molecule (PSA-NCAM; an immature neuron marker), β3-tubulin (axonal marker) and GAP 43, were markedly increased in the hypertrophied right ventricles, in parallel with NGF upregulation. Thus, the ET-1/NGF pathway contributes to anatomical sympathetic hyperinnervation in pressure overload-induced cardiac hypertrophy. Given that ET-1 is strongly induced in myocardial infarction, the ET-1/NGF pathway may also be involved in NGF upregulation and nerve regeneration after myocardial infarction.

NERVE GROWTH FACTOR IS CRITICAL FOR CARDIAC SENSORY INNERVATION AND RESCUES NEUROPATHY IN DIABETIC HEARTS

The cardiac autonomic nervous system is composed of efferent and afferent nerves. The cardiac sensory nervous system is responsible for pain perception and for initiating a protective cardiovascular response during myocardial ischemia [18, 19, 46, 47]. Cardiac sensory nerve impairment causes silent myocardial ischemia, which

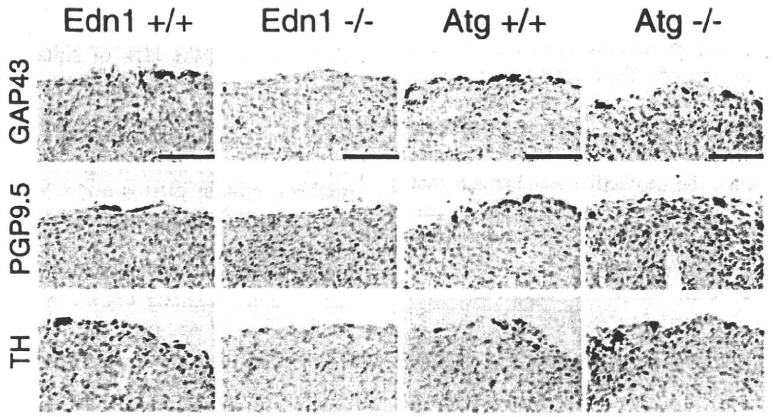

Fig. (1). Disruption of ET-1, but not of angiotensinogen, reduces sympathetic nerve density in murine hearts.

Immunostaining for GAP43, PGP9.5, and TH in the heart. Note that GAP43-, PGP9.5-, and TH-immunopositive nerves are detected less frequently in *Edn1*$^{-/-}$ mice, but not in *Atg*$^{-/-}$ mice, as compared to the respective WT littermates. Scale bar, 100 μm.

is a major cause of sudden death in DM patients [12]. Despite the severity of this complication, the alterations in cardiac sensory innervation and the molecular mechanism that underlies sensory neuropathy in diabetic hearts are poorly understood [48-53]. Moreover, little is known about the anatomical distribution of cardiac sensory nerves and the molecular mechanism of innervation during development [54].

Unlike somatic tissues, visceral organs, such as the heart, are believed to be rich in autonomic efferent innervation but poor in nociceptive afferent nerves [55]. In fact, Zahner *et al.* [56] have reported that vanilloid receptor-1-immunopositive sensory nerves are enriched in the epicardium but scarce in the myocardium. We have identified for the first time that cardiac sensory innervation is rich not only at epicardial sites but also in the ventricular myocardium, and that sensory innervation increases with development [21, 57]. In our screen of several neurotrophic factors, we have found that cardiac sensory nerves develop in parallel with NGF synthesized in the heart [58]. Cardiac nociceptive sensory nerves that are immunopositive for CGRP, the dorsal root ganglia, and the dorsal horn are markedly retarded in NGF-deficient mice, while cardiac-specific overexpression of NGF rescues these deficits. Thus, NGF synthesis in the heart is critical for the development of the cardiac sensory nervous system [59].

To investigate whether NGF is involved in diabetic neuropathy, DM was induced with streptozotocin in wild-type (WT) and transgenic mice that overexpressed NGF in the heart [21, 60-63]. Downregulation of NGF, CGRP-immunopositive cardiac sensory denervation, and atrophic changes in dorsal root ganglia were observed in DM-induced WT mice, whereas these deteriorations were rescued in DM-induced NGF-transgenic mice (Fig. **2**). Cardiac sensory function, as measured by myocardial ischemia-induced c-Fos expression in dorsal root ganglia, was also downregulated by DM in the WT mice, but not in the NGF-transgenic mice [19]. Direct gene transfer of NGF into the diabetic rat hearts improved the impaired cardiac sensory innervation and function, as determined by the electrophysiological activities of cardiac afferent nerves during myocardial ischemia [64, 65]. These findings demonstrate that the development of the cardiac sensory nervous system is dependent on NGF synthesized in the heart, and that DM-induced NGF reduction may lead to cardiac sensory neuropathy.

Phase I and phase II clinical trials of systemic administration of recombinant NGF have revealed safety and potential efficacy in diabetic polyneuropathy, although a phase III trial did not show beneficial effects, as the dosage and route of administration may have been suboptimal [66, 67]. The dosage of NGF was restricted by side-effects, and the development of anti-NGF antibodies may have contributed to the lack of beneficial effects in the phase III clinical trial. These complications might be avoided by directly administering the *NGF* gene to the cells that require the factor. NGF- and CGRP-immunopositive nerves were proportionally reduced in diabetic hearts, and thus we successfully treated cardiac sensory neuropathy by direct *NGF* gene transfer. Consistent with our findings, the efficacy of *NGF* gene therapy has been reported in diabetic cystopathy and neuropathy of the footpad [67, 68]. Further studies on the reliability and efficacy of this gene therapy are required before clinical trials can proceed.

SEMA3A IS CRITICAL FOR CARDIAC SYMPATHETIC INNERVATION PATTERNING

As discussed above, NGF plays critical roles in cardiac nerve development. In contrast, the neural chemorepellent that induces growth-cone collapse and repels nerve axons has not been identified in the heart. *Sema3a*, which is a Class 3 secreted semaphorin, has been cloned and identified as a potent neural chemorepellent and a directional guidance molecule for nerve fibers [69-71]. However, it is not known whether cardiomyocytes produce Sema3a, and if so, whether this protein affects sympathetic neural patterning and cardiac performance.

We analyzed the kinetics and distribution of cardiac sympathetic innervation in developing murine ventricles [22]. TH-immunopositive sympathetic nerve endings appeared on the epicardial surface at embryonic day (E)15, and gradually increased in number in the myocardium after postnatal day (P)7 and P42. In the ventricular myocardium, sympathetic nerves were found to be more abundant in the subepicardium than in the subendocardium, suggesting an epicardial-to-endocardial gradient [1, 4, 15, 16]. To identify the *Sema3a* expression pattern and its relationship to innervation patterning in the heart, we analyzed heterozygous *Sema3a* knocked-in *lacZ* mice ($Sema3a^{lacZ/+}$). At E12, *lacZ* expression was detected strongly in the heart, especially in the trabecular components of the ventricles. In E15 hearts, *lacZ* expression was observed in the subendocardium but not in the subepicardium of the atria and ventricles. At P1 and P42, *lacZ* expression was reduced in certain regions and highlighted the Purkinje fiber network along the ventricular free wall [72, 73]. Quantitative RT-PCR of *Sema3a* in developing hearts also revealed the presence of *Sema3a* from E12, with subsequent linear decrease in expression, in contrast to the pattern of sympathetic innervation. These results indicate that Sema3a shows the opposite kinetics and distribution pattern of expression to the pattern of sympathetic innervation in developing

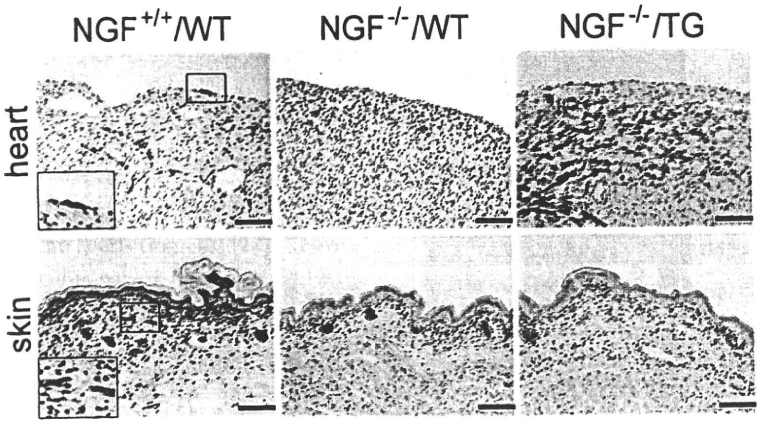

Fig. (2). Cardiac-specific overexpression of NGF rescues the cardiac sensory nervous system defects in NGF-deficient mice.
Immunostaining for CGRP in the hearts and limb skin of $NGF^{+/+}/WT$, $NGF^{-/-}/WT$, and $NGF^{-/-}/TG$ mice. Note that $NGF^{-/-}/TG$ hearts are hyperinnervated compared to $NGF^{-/-}/WT$ littermates. In contrast, there are no differences in skin denervation. Scale bar, 100 μm.

hearts, which suggests that Sema3a negatively regulates cardiac innervation (Fig. 3).

To investigate whether Sema3a is critical for cardiac sympathetic nerve development, we analyzed *Sema3a*-deficient mice (*Sema3a*$^{-/-}$) [74, 75]. The WT hearts showed a clear epicardial-to-endocardial gradient of sympathetic innervation. In contrast, the sympathetic nerve density was reduced in the subepicardium but increased in the subendocardium of *Sema3a*$^{-/-}$ mice, resulting in disruption of the innervation gradient in *Sema3a*$^{-/-}$ ventricles. The *Sema3a*$^{-/-}$ mice also exhibited malformation of the stellate ganglia that extend sympathetic nerves to the heart. To investigate whether the abnormal sympathetic innervation patterning in *Sema3a*$^{-/-}$ hearts is a secondary effect of stellate ganglia malformation, we generated transgenic mice that overexpressed *Sema3a* specifically in the heart (*SemaTG*) [76]. *SemaTG* mice were associated with reduced sympathetic innervation and attenuation of the epicardial-to-endocardial innervation gradient. These results indicate that cardiomyocyte-derived Sema3a plays critical roles in cardiac sympathetic innervation by inhibiting neural growth. Since cardiomyocyte-derived NGF acts as a chemoattractant, it is possible that the balance between NGF and Sema3a synthesized in the heart determines cardiac sympathetic innervation patterning.

The growth-cone behavior of somatic sensory axons is also modulated by coincident signaling between NGF and Sema3a [77, 78]. During development, NGF and Sema3a are expressed within the spinal cord and influence the pathway guidance of sensory axons. Sema3a is specifically expressed in the ventral half of the spinal cord and mediates NGF-responsive sensory axons to terminate at the dorsal part of the spinal cord [69, 79]. Targeted inactivation of *Sema3a* disrupts neural patterning and projections in the spinal cord, which underscores the importance of Sema3a signaling for the directional guidance of nerve fibers [74, 75].

SEMA3A MAINTAINS ARRHYTHMIA-FREE HEARTS THROUGH SYMPATHETIC INNERVATION PATTERNING

Most of the *Sema3a*$^{-/-}$ mice died within the first postnatal week, with only 20% surviving viable until weaning [74, 75]. To identify the cause of death and the effects of abnormal sympathetic neural distribution in *Sema3a*$^{-/-}$ hearts, we performed telemetric electrocardiography and heart-rate variability analysis [80, 81]. In addition to multiple premature ventricular contractions, *Sema3a*$^{-/-}$ mice developed sinus bradycardia and abrupt sinus arrest due to sympathetic neural dysfunction.

The *SemaTG* mice died suddenly without any symptoms at10 months of age. Sustained ventricular tachyarrhythmia was induced in *SemaTG* mice but not in WT mice after epinephrine administration, and programmed electrical stimulation revealed that *SemaTG* mice were highly susceptible to ventricular tachyarrhythmia [82, 83]. The β1-adrenergic receptor density was upregulated and the cAMP response after catecholamine injection was exaggerated in *SemaTG* ventricles. Action potential duration was significantly prolonged in hypoinnervated *SemaTG* ventricles, presumably *via* ion channel modulation. These results suggest that the higher susceptibility of *SemaTG* mice to ventricular arrhythmia is due at least in part to catecholamine supersensitivity and prolongation of action potential duration, both of which can augment triggered activity in cardiomyocytes [84-88]. Thus, Sema3a-mediated sympathetic innervation patterning is critical for the maintenance of arrhythmia-free hearts.

Sympathetic nerves modulate the function of ion channels and trigger various arrhythmias in diseased hearts [10, 11]. However, the relationship between sympathetic innervation and arrhythmogenicity in structurally normal hearts has been unclear. Induction of sympathetic hyperinnervation in normal adult canine hearts by either NGF infusion or subthreshold electrical stimulation of the left stellate ganglion resulted in no arrhythmia except for sinus tachycardia. However, the same magnitude of sympathetic hyperinnervation in diseased hearts cause increased incidence and sudden death [5]. These findings suggest that sympathetic hyperinnervation in normal canine hearts are not arrhythmogenic. On the other hand, the *Sema3a*$^{-/-}$ mice exhibited sinus bradycardia, abrupt sinus slowing, and stellate ganglia defects. Consistent with our data, right stellectomy has been shown to induce sinus bradycardia and sudden, asystolic death in dogs [89]. In addition, Stramba-Badiale *et al.* [90] have reported that a developmental abnormality in cardiac innervation may play a role in the genesis of some cases of sudden infant death syndrome. Thus, the onset and duration of sympathetic neural dysfunction might be critical for arrhythmogenicity in structurally normal hearts. The *SemaTG* hearts were also highly susceptible to ventricular arrhythmias, albeit without contractile dysfunc-

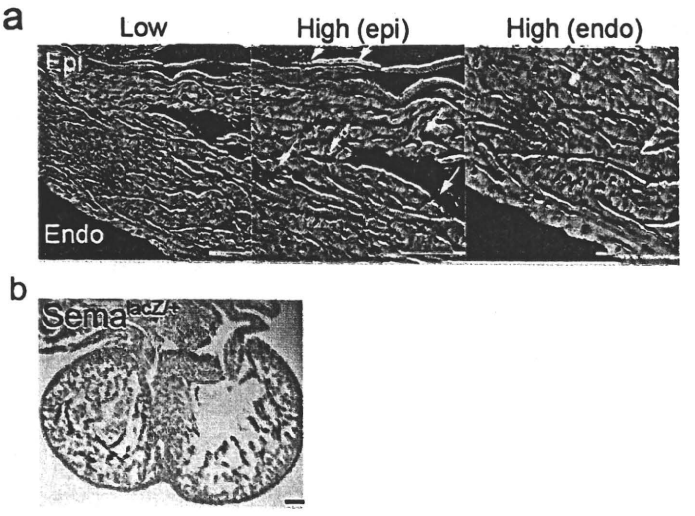

Fig. (3). Inverse expression pattern of *Sema3a* and sympathetic innervation in murine hearts.

(**a**) Immunofluorescence staining for α-actinin (red), TH (green), and TOTO-3 (blue, nuclei). TH-immunopositive nerves (arrows) are more abundant in the subepicardium (Epi) than in the subendocardium (Endo). Low and High indicate low-power and high-power magnification fields, respectively. (**b**) X-gal staining (green) of *Sema3a*$^{lacZ/+}$ hearts at E12 demonstrates strong *Sema3a* expression in the subendocardium. Scale bar, 100 μm.